IOP Publishing Physica Scripta
Phys. Scr. 95 (2020) 035221 (22pp) https://doi.org/10.1088/1402-4896/ab43b6

On the nonlocality of bilateral vibrations of single-layered membranes from vertically aligned double-walled carbon nanotubes

Keivan Kiani and Hossein Pakdaman

Department of Civil Engineering, K.N. Toosi University of Technology, Valiasr Ave., P.O. Box 15875-4416, Tehran, Iran

E-mail: k_kiani@kntu.ac.ir and keivankiani@yahoo.com

Received 25 July 2019, revised 3 September 2019
Accepted for publication 11 September 2019
Published 6 February 2020

Abstract

Through developing constructive nonlocal models, both in- and out-of-plane free dynamic analyses of single-layered of double-walled carbon nanotubes (DWCNTs) are going to be investigated carefully. By exploiting the nonlocal Rayleigh and Timoshenko beams, the rigorous governing equations of the nanosystem that explicitly express its transverse vibrations are extracted by continuum-based simulating the van der Waals forces. The abilities of the nonlocal continuous-based models in estimating the results of the nonlocal discrete-based models are proved. Afterward, the nonlocal transverse frequencies are evaluated and the roles of influential factors plus to the shear effect on the free dynamical response are elucidated and discussed methodically. The obtained results from this scrutiny provide a reasonably smooth path for inspecting mechanical behavior of more complex systems composed of vertically aligned DWCNTs.

Supplementary material for this article is available online

Keywords: bilateral vibrations, membranes of double-walled carbon nanotubes, interactional van der Waals forces, nonlocal discrete and continuous modeling, nonlocal beams, assumed mode method

1. Introduction

To prepare two-dimensional surface regions via carbon nanotubes (CNTs), in which would have great applications in supercapacitors [1–3], fuel cells [4–6], and field emission [7, 8], it is required to synthesize or relocate CNTs onto a suitable surface appropriately until shaping the paper-like building with preferred thickness. As a genius solution, double-walled carbon nanotubes (DWCNTs) could be exploited for such purposes. In recent years, these tiny nanostructures have attracted numerous research interests owing to their brilliant mechanical, electrical, and thermal properties as well as unique coaxial architecture compared to single-walled or even multi-walled carbon nanotubes (SWCNTs or MWCNTs) [9–13]. On the other hand, the experimentally observed data confirms this fact that the mechanical behavior of the resulting assembly is generally enhanced by aligning the nanotubes [14, 15]. In these views, herein, the authors are encouraged to explore free vibrations of single-layered membranes consisting of vertically aligned DWCNTs.

The classical continuum theory could not be used for modeling of nanostructures since the interatomic bonds do not incorporated into the constitutive relations as well as equations of motion. For elasticity-based modeling of each CNT, we employ the nonlocal theory of continuum mechanics (NTC) of Eringen [16–19]. According to the NTC, the stress state of each point depends on the stress states of that point as well as those of adjacent points. This critical concept is called *nonlocality* and the nonlocal stresses are defined by the integral of product of an appropriate kernel function by the corresponding classical stresses over the space domain of the structure. The aforementioned kernel functions have compact support controlled by the small-scale factor. This parameter has been calibrated for both SWCNTs [20, 21] and DWCNTs [22]

through performing appropriate atomic simulations. The above-mentioned integro-differential version of the NTC has been of focus of attention of investigators during recent years [23, 24]; however, we employ the differential version of this theory in this paper, and application of the integro-differential type of this theory to the present problem can be considered as a complementary scrutiny for future works. It is noticed that the differential-based formulations of the Eringen's NTC have been broadly exploited for mechanical modeling of nanorods [25, 26], nanobeams [27, 28] and nanoplates [29–31].

Up to now, various mechanical aspects of SWCNTs and their composites have been investigated [32–40]. Concerning mechanical behavior of DWCNTs, mostly in the context of the NTC, their free dynamics [41–45], free vibrations under action of magnetic field [46–49], elastic buckling [50–52], nonlinear buckling [53, 54], forced vibrations [55], and nonlinear vibrations [56, 57] have been broadly studied. Additionally, buckling and free vibrations of membranes and three-dimensional ensembles from SWCNTs have been examined using nonlocal beam theories [58–61]. However, free transverse vibrational behavior of elastically embedded membranes from DWCNTs has not been explored yet.

Herein, we exploit the nonlocal Rayleigh and Timoshenko beam models (NRBM and NTBM) for mechanical modeling of constitutive vertically aligned DWCNTs of the nanosystem. To take into account the van der Waals (vdW) forces between the consisting atoms of the inside tube and those of the outside tube as well as the vdW forces between the atoms of doubly near DWCNTs, these are simulated by linearly continuous elastic springs. To consider the lateral interactions of the nanosystem with its neighboring medium, Pasternak-type foundation model is implemented. For an arbitrary number of DWCNTs, the nonlocal transverse motion equations are derived via both NRBM and NTBM. These are commonly called *discrete models* since the governing equations should be constructed for each tube individually accounting for the vdW forces. To get rid of the number of DWCNTs in dynamic analysis of the problem, we also develop several useful *continuous models*. It will be shown that these models can effectively describe overall dynamic behavior of the nanosystem, irrespective of vibration of every particular DWCNT. Several constructive numerical studies are carried out, and the influences of the important factors including the nonlocal and shear effects on the free dynamic response in both lateral directions are studied carefully. The proposed models as well as the methodologies in their vibrational analyses would be very beneficial in scrutinizing vibrations of more complicated configurations such as multi-layered and orthogonal-layered membranes from vertically aligned DWCNTs. The dynamic analyses of these of our interest structural forms can be followed by curious investigators in the near future.

2. Vibrational scrutiny using nonlocal discrete models

In figure 1(a), the vertically aligned DWCNTs of a single-layered membrane confined by an elastic matrix have been demonstrated schematically. The length of consisting tubes is denoted by l_b, the thickness of the wall of the continuum-based tubes is represented by th while the intertube distance of two neighboring DWCNTs is denoted by d. For each DWCNTs, the mean radius of the inner nanotube is represented by r_{m_1} while that of the outer nanotube is $r_{m_1} + th$. For continuum-based modeling of the interactive vdW pressures between the consisting atoms of the neighboring tubes, we utilize linear virtual springs of constants $S_{vy_{(m,n)}}$ and $S_{vz_{(m,n)}}$ according to the given formulations in the next part. Additionally, the dynamic interactions of the outermost tubes with the nearby matrix are allowed by the Pasternak foundation model, in which the stiffness of the lateral is K_t while the rotational spring's stiffness is represented by K_r (see figure 1(b)).

In the present work, we are extremely interested in developing elasticity-based models to examine free vibrations of such nanosystems. For this purpose, appropriate nonlocal models are constructed and explained. More specifically, in the upcoming discrete models, the bidirectional deflections of any tube would be coupled with those of other ones due to the rigorous vdW forces. Hence, for a membrane with a high number of DWCNTs, the needed computations as well as the labor expenditures would be high enough. To resolve this major fault of the discrete models, we will establish several nonlocal continuous models as well. In such models, all the lateral deformation fields of all nanotubes are expressed by just two continuous deflection fields. Therefore, it is expected that the number of consisting nanotubes of the nanosystem would have a trivial influence on the aforementioned costs. With regard to this fact that only transverse vibrations of vertically aligned membranes are of particular concern, we implement the NRBM and NTBM for capturing the free dynamic response of such nanosystems.

2.1. On the continuum-based modeling of vdW forces between two DWCNTs

The Lennard–Jones potential function could appropriately explain the interactional forces between two neutral atoms, given by: $\Phi(r) = 4\epsilon\left[\left(\frac{\sigma}{r}\right)^{12} - \left(\frac{\sigma}{r}\right)^{6}\right]$, where ϵ denotes the depth of the well, σ is displayed by $\frac{r_a}{\sqrt[6]{2}}$, in which r_a is the inter-particle distance associated with the equilibrium state, and r represents the inter-particle distance. By taking the first derivative of the potential function, the vdW force between the ith and jth atoms is provided by:

$$\overrightarrow{f_{ji}} = F_{y_{ji}}e_y + F_{z_{ji}}e_z = -\frac{\mathrm{d}\Phi}{\mathrm{d}r}e_r = \frac{24\epsilon}{\sigma^2}\left[2\left(\frac{\sigma}{r}\right)^{14} - \left(\frac{\sigma}{r}\right)^{8}\right]\overrightarrow{r_{ji}}, \quad (1)$$

in which $\overrightarrow{r_{ji}}$ denotes the relative position vector, and $\mathbf{e}_r$ is the corresponding unit vector. According to the provided figure 2, the position vector of an atom from a tube of the lhs DWCNTs and that of the rhs one is written as in the

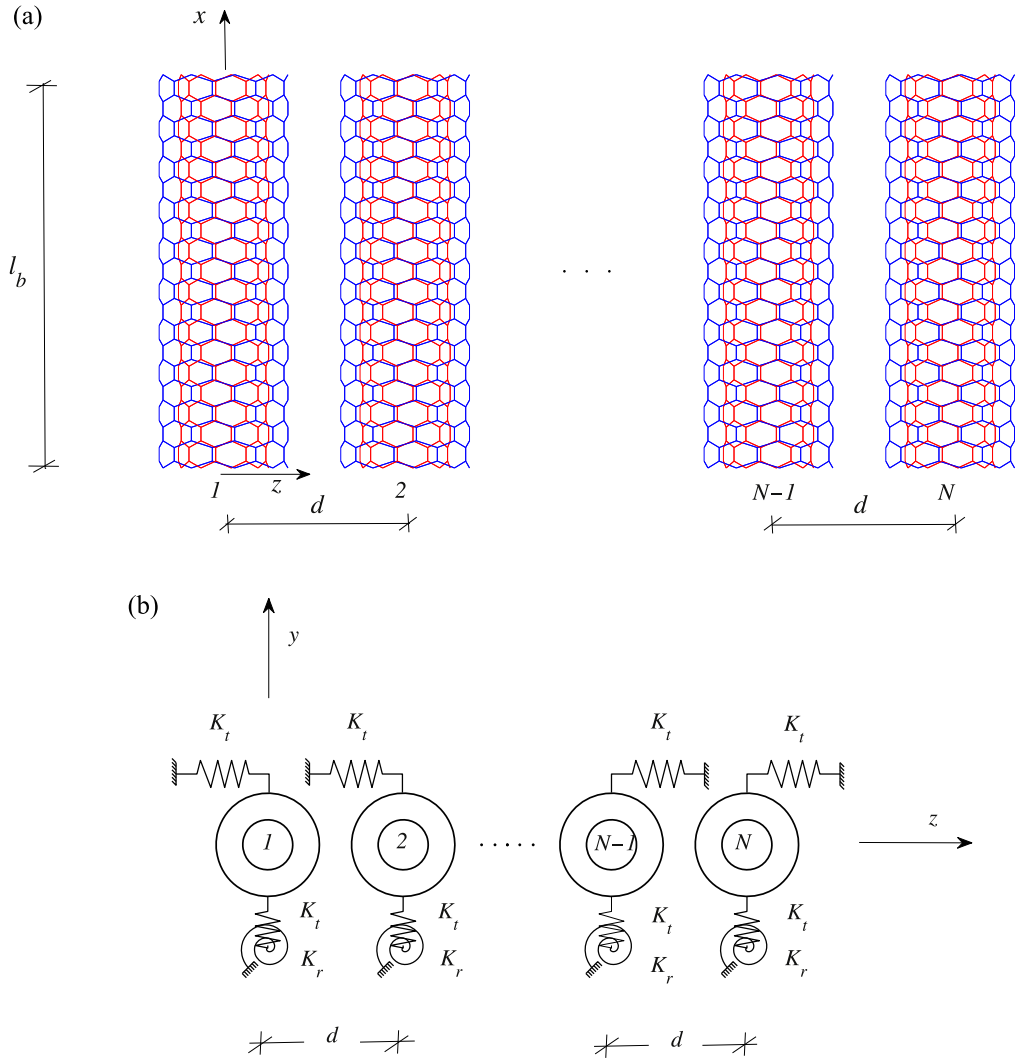

Figure 1. A membrane made from multiple neighboring DWCNTs embedded in an matrix: (a) side view of the nanosystem, (b) cross-sectional view of the continuum-based structure.

cylindrical coordinate system:

$$\overrightarrow{r_{ji}} = (x_j - x_i)\mathbf{e}_x + (r_{m_j}\cos(\phi_j) - r_{m_i}\cos(\phi_i) - \Delta\mathcal{V}_{ji})\mathbf{e}_y + (r_{m_j}\sin(\phi_j) - r_{m_i}\sin(\phi_i) + d - \Delta\mathcal{W}_{ji})\mathbf{e}_z, \quad (2)$$

where r_{m_j} and r_{m_i} are the mean radius of the constitutive tubes of DWCNTs such that $(j, i) = (3, 1), (3, 2), (4, 1), (4, 2)$. On the other hand, for each DWCNTs, by denoting the location of the kth atom of the outermost tube by $(x_k, r_{m_k}\cos(\phi_k), r_{m_k}\sin(\phi_k))$ and the location of the lth atom of the innermost tube by $(x_l, r_{m_l}\cos(\phi_l), r_{m_l}\sin(\phi_l))$, the relative position vector is expressed by:

$$\overrightarrow{r_{kl}} = (x_k - x_l)\mathbf{e}_x + (r_{m_k}\cos(\phi_k) - r_{m_l}\cos(\phi_l) - \Delta\mathcal{V}_{kl})\mathbf{e}_y + (r_{m_k}\sin(\phi_k) - r_{m_l}\sin(\phi_l) - \Delta\mathcal{W}_{kl})\mathbf{e}_z, \quad (3)$$

in which $(k, l) = (2, 1), (4, 3)$, r_{m_k} and r_{m_l} in order are the mean radius of the innermost and outermost tubes, $(\Delta\mathcal{V}_{mn}, \Delta\mathcal{W}_{mn}) = (\mathcal{V}_m^{[.]} - \mathcal{V}_n^{[.]}, \mathcal{W}_m^{[.]} - \mathcal{W}_n^{[.]})$, where $\mathcal{V}_i^{[.]} = \mathcal{V}_i^{[.]}(x, t)$ and $\mathcal{W}_i^{[.]} = \mathcal{W}_i^{[.]}(x, t)$; $[.] = R$ or T in order are the dynamic transverse displacements associated with the y and z directions (see figure 2). Using equations (1)–(3), the components of existing vdW forces between innermost–innermost, outermost–outermost, and innermost–outermost

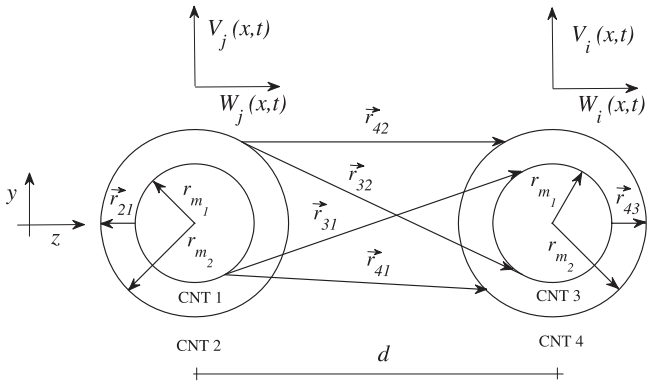

Figure 2. A representation of doubly adjacent DWCNTs for evaluating the rigorous vdW forces.

tubes are stated by:

$$F_{y_{ji}} = \frac{24\epsilon\sigma_{\mathrm{CNT}}^2 r_{m_j} r_{m_i}}{l_b \sigma^2} \int_0^{l_b}\int_0^{l_b}\int_0^{2\pi} \times \int_0^{2\pi}\left[2\left(\frac{\sigma}{\lambda}\right)^{14} - \left(\frac{\sigma}{\lambda}\right)^{8}\right] \times (r_{m_j}\cos(\phi_j) - r_{m_i}\cos(\phi_i) - \Delta\mathcal{V}_{ji}) \times \mathrm{d}\phi_j \mathrm{d}\phi_i \mathrm{d}x_j \mathrm{d}x_i, \tag{4a}$$

$$F_{z_{ji}} = \frac{24\epsilon\sigma_{\mathrm{CNT}}^2 r_{m_j} r_{m_i}}{l_b \sigma^2} \int_0^{l_b}\int_0^{l_b}\int_0^{2\pi} \times \int_0^{2\pi}\left[2\left(\frac{\sigma}{\lambda}\right)^{14} - \left(\frac{\sigma}{\lambda}\right)^{8}\right] \times (r_{m_j}\sin(\phi_j) - r_{m_i}\sin(\phi_i) + \mathrm{d} - \Delta\mathcal{W}_{ji}) \times \mathrm{d}\phi_j \mathrm{d}\phi_i \mathrm{d}x_j \mathrm{d}x_i, \tag{4b}$$

$$F_{y_{kl}} = \frac{24\epsilon\sigma_{\mathrm{CNT}}^2 r_{m_k} r_{m_l}}{l_b \sigma^2} \int_0^{l_b}\int_0^{l_b}\int_0^{2\pi} \times \int_0^{2\pi}\left[2\left(\frac{\sigma}{\lambda}\right)^{14} - \left(\frac{\sigma}{\lambda}\right)^{8}\right] \times (r_{m_k}\cos(\phi_k) - r_{m_l}\cos(\phi_l) - \Delta\mathcal{V}_{kl}) \times \mathrm{d}\phi_k \mathrm{d}\phi_l \mathrm{d}x_k \mathrm{d}x_l, \tag{4c}$$

$$F_{z_{kl}} = \frac{24\epsilon\sigma_{\mathrm{CNT}}^2 r_{m_k} r_{m_l}}{l_b \sigma^2} \int_0^{l_b}\int_0^{l_b}\int_0^{2\pi} \times \int_0^{2\pi}\left[2\left(\frac{\sigma}{\lambda}\right)^{14} - \left(\frac{\sigma}{\lambda}\right)^{8}\right] \times (r_{m_k}\sin(\phi_l) - r_{m_l}\sin(\phi_l) - \Delta\mathcal{W}_{kl}) \times \mathrm{d}\phi_k \mathrm{d}\phi_l \mathrm{d}x_k \mathrm{d}x_l, \tag{4d}$$

where $\sigma_{\mathrm{CNT}} = \frac{4\sqrt{3}}{9a^2}$ and a denotes the C–C bond's length. In order to estimate the rigorous vdW forces, the Taylor series of such statements up to the first-order are provided by:

$$F_{y_{(mn)}} \approx F_{y_{(mn)}}(\Delta\mathcal{V}_{mn} = 0) + \Delta F_{y_{(mn)}}; \quad \Delta F_{y_{mn}} = S_{vy_{(m,n)}}\Delta\mathcal{V}_{mn}, \tag{5a}$$

$$F_{z_{mn}} \approx F_{z_{mn}}(\Delta\mathcal{W}_{mn} = 0) + \Delta F_{z_{mn}}; \quad \Delta F_{z_{mn}} = S_{vz_{(m,n)}}\Delta\mathcal{W}_{mn}, \tag{5b}$$

in these relations, $F_{y_{(mn)}}(\Delta\mathcal{V}_{mn} = 0)$ and $F_{z_{mn}}(\Delta\mathcal{W}_{mn} = 0)$ in order are the components of the static vdW forces pertinent to the y-axis and the z-axis, $\Delta F_{y_{mn}}$ and $\Delta F_{z_{mn}}$ represent the change in the vdW forces due to the relative deflection of the mth tube wrt the nth one associated with the y and z directions, respectively. In view of equations (5*a*) and (5*b*), we can employ linear-continuous springs for simulating the rigorous vdW forces between consisting atoms of two nearby tubes. The coefficients associated with the change of the vdW interactional forces because of the relative lateral motions of the adjacent walls are then computed by:

$$S_{vy_{(j,i)}} = \frac{-256\epsilon\, r_{m_j} r_{m_i}}{9a^4 l_b} \int_0^{l_b}\int_0^{l_b}\int_0^{2\pi} \times \int_0^{2\pi}\left\{\begin{array}{l}\sigma^{12}\left[\chi_1^{-7} - 14\chi_1^{-8}\left(\begin{array}{c} r_{m_j}\cos(\phi_j) - \\ r_{m_i}\cos(\phi_i)\end{array}\right)^2\right] \\ -\frac{\sigma^6}{2}\left[\chi_1^{-4} - 8\chi_1^{-5}\left(\begin{array}{c} r_{m_j}\cos(\phi_j) - \\ r_{m_i}\cos(\phi_i)\end{array}\right)^2\right]\end{array}\right\} \times \mathrm{d}\phi_j \mathrm{d}\phi_i \mathrm{d}x_j \mathrm{d}x_i, \tag{6a}$$

$$S_{vz_{(j,i)}} = \frac{-256\epsilon\, r_{m_j} r_{m_i}}{9a^4 l_b} \int_0^{l_b}\int_0^{l_b}\int_0^{2\pi} \times \int_0^{2\pi}\left\{\begin{array}{l}\sigma^{12}\left[\chi_1^{-7} - 14\chi_1^{-8}\left(\begin{array}{c} r_{m_j}\sin(\phi_j) - \\ r_{m_i}\sin(\phi_i) + d\end{array}\right)^2\right] \\ -\frac{\sigma^6}{2}\left[\chi_1^{-4} - 8\chi_1^{-5}\left(\begin{array}{c} r_{m_j}\sin(\phi_j) - \\ r_{m_i}\sin(\phi_i) + d\end{array}\right)^2\right]\end{array}\right\} \times \mathrm{d}\phi_j \mathrm{d}\phi_i \mathrm{d}x_j \mathrm{d}x_i, \tag{6b}$$

$$S_{vy_{(k,l)}} = \frac{-256\epsilon\, r_{m_k} r_{m_l}}{9a^4 l_b} \int_0^{l_b}\int_0^{l_b}\int_0^{2\pi} \times \int_0^{2\pi}\left\{\begin{array}{l}\sigma^{12}\left[\chi_2^{-7} - 14\chi_2^{-8}\left(\begin{array}{c} r_{m_k}\cos(\phi_k) - \\ r_{m_l}\cos(\phi_l)\end{array}\right)^2\right] \\ -\frac{\sigma^6}{2}\left[\chi_2^{-4} - 8\chi_2^{-5}\left(\begin{array}{c} r_{m_k}\cos(\phi_k) - \\ r_{m_l}\cos(\phi_l)\end{array}\right)^2\right]\end{array}\right\} \times \mathrm{d}\phi_k \mathrm{d}\phi_l \mathrm{d}x_k \mathrm{d}x_l, \tag{6c}$$

$$S_{vz_{(k,l)}} = \frac{-256\epsilon\, r_{m_k} r_{m_l}}{9a^4 l_b} \int_0^{l_b}\int_0^{l_b}\int_0^{2\pi} \times \int_0^{2\pi}\left\{\begin{array}{l}\sigma^{12}\left[\chi_2^{-7} - 14\chi_2^{-8}\left(\begin{array}{c} r_{m_k}\sin(\phi_k) - \\ r_{m_l}\sin(\phi_l)\end{array}\right)^2\right] \\ -\frac{\sigma^6}{2}\left[\chi_2^{-4} - 8\chi_2^{-5}\left(\begin{array}{c} r_{m_k}\sin(\phi_k) - \\ r_{m_l}\sin(\phi_l)\end{array}\right)^2\right]\end{array}\right\} \times \mathrm{d}\phi_k \mathrm{d}\phi_l \mathrm{d}x_k \mathrm{d}x_l, \tag{6d}$$

where $\chi_1 = \chi_1(x_j, x_i, \phi_j, \phi_i; r_{m_j}, r_{m_i}, d)$ and $\chi_2 = \chi_2(x_j, x_i, \phi_j, \phi_i; r_{m_j}, r_{m_i})$ are as:

$$\chi_1 = (x_j - x_i)^2 + (r_{m_j}\cos(\phi_j) - r_{m_i}\cos(\phi_i))^2 + (r_{m_j}\sin(\phi_j) - r_{m_i}\sin(\phi_i) + d)^2, \tag{7a}$$

$$\chi_2 = (x_k - x_l)^2 + (r_{m_k}\cos(\phi_k) - r_{m_l}\cos(\phi_l))^2 + (r_{m_k}\sin(\phi_k) - r_{m_l}\sin(\phi_l))^2. \tag{7b}$$

2.2. Application of the NRBM for discrete modeling of membranes of DWCNTs

2.2.1. Nonlocal-discrete equations of motion. To derive the nonlocal governing equations pertinent to transverse vibrations, the principle of Hamilton is planned to be implemented. For this purpose, the kinetic energy of the single-layered multiple DWCNTs as well as its strain energy should be carefully expressed.

By exploitation of the NRBM, the kinetic energy of the nanosystem is given by:

$$T^R(t)=\frac{1}{2}\sum_{i=1}^{2N}\int_0^{l_b}\rho_{b_i}\left(A_{b_i}\left(\left(\frac{\partial \mathcal{V}_i^R}{\partial t}\right)^2+\left(\frac{\partial \mathcal{W}_i^R}{\partial t}\right)^2\right)+I_{b_i}\left(\left(\frac{\partial^2 \mathcal{V}_i^R}{\partial t\partial x}\right)^2+\left(\frac{\partial^2 \mathcal{W}_i^R}{\partial t\partial x}\right)^2\right)\right)\mathrm{d}x, \tag{8}$$

where ρ_{b_i} is the density, I_{b_i} is the cross-sectional moment inertia, and A_{b_i} is the cross-sectional area of the equivalent continuum structure (ECS) associated with the ith tube. Furthermore, by considering the rigorous vdW pressures as well as the transverse dynamical interactions of the nanosystem with the adjoining matrix based on the NRBM, the whole nonlocal strain energy of the single-layered membrane made from DWCNTs can be formulated by:

$$\begin{aligned}U^R(t)=&\frac{1}{2}\sum_{i=1}^{2N}\int_0^{l_b}\left[-\frac{\partial^2 \mathcal{V}_i^R}{\partial x^2}(M_{bz_i}^{nl})^R-\frac{\partial^2 \mathcal{W}_i^R}{\partial x^2}(M_{by_i}^{nl})^R\right]\mathrm{d}x\\
&+\frac{1}{2}\sum_{i=2,4,\ldots}^{2N}\int_0^{l_b}\left[\begin{array}{c}S_{vy_{(i,i-1)}}(\mathcal{V}_i^R-\mathcal{V}_{i-1}^R)^2+S_{vy_{(i,i+2)}}(\mathcal{V}_i^R-\mathcal{V}_{i+2}^R)^2(1-\delta_{(2N)(i)})\\
+S_{vy_{(i,i+1)}}(\mathcal{V}_i^R-\mathcal{V}_{i+1}^R)^2(1-\delta_{(2N)(i)})+S_{vy_{(i,i-2)}}(\mathcal{V}_i^R-\mathcal{V}_{i-2}^R)^2(1-\delta_{2i})\\
+S_{vy_{(i,i-3)}}(\mathcal{V}_i^R-\mathcal{V}_{i-3}^R)^2(1-\delta_{2i})+K_t(\mathcal{V}_i^R)^2+K_r\left(\frac{\partial \mathcal{V}_i^R}{\partial x}\right)^2\end{array}\right]\mathrm{d}x\\
&+\frac{1}{2}\sum_{i=3,5\ldots}^{2N-1}\int_0^{l_b}\left[\begin{array}{c}S_{vy_{(i,i+1)}}(\mathcal{V}_i^R-\mathcal{V}_{i+1}^R)^2+S_{vy_{(i,i+2)}}(\mathcal{V}_i^R-\mathcal{V}_{i+2}^R)^2(1-\delta_{(2N-1)(i)})+\\
S_{vy_{(i,i+3)}}(\mathcal{V}_i^R-\mathcal{V}_{i+3}^R)^2(1-\delta_{(2N-1)(i)})+S_{vy_{(i,i-2)}}(\mathcal{V}_i^R-\mathcal{V}_{i-2}^R)^2(1-\delta_{1i})\\
+S_{vy_{(i,i-1)}}(\mathcal{V}_i^R-\mathcal{V}_{i-1}^R)^2(1-\delta_{1i})\end{array}\right]\mathrm{d}x\\
&+\frac{1}{2}\sum_{i=2,4,\ldots}^{2N}\int_0^{l_b}\left[\begin{array}{c}S_{vz_{(i,i-1)}}(\mathcal{W}_i^R-\mathcal{W}_{i-1}^R)^2+S_{vz_{(i,i+2)}}(\mathcal{W}_i^R-\mathcal{W}_{i+2}^R)^2(1-\delta_{(2N)(i)})\\
+S_{vz_{(i,i+1)}}(\mathcal{W}_i^R-\mathcal{W}_{i+1}^R)^2(1-\delta_{(2N)(i)})+\\
S_{vz_{(i,i-2)}}(\mathcal{W}_i^R-\mathcal{W}_{i-2}^R)^2(1-\delta_{2i})+S_{vz_{(i,i-3)}}(\mathcal{W}_i^R-\mathcal{W}_{i-3}^R)^2(1-\delta_{2i})\\
+K_t(\mathcal{W}_i^R)^2+K_r\left(\frac{\partial \mathcal{W}_i^R}{\partial x}\right)^2\end{array}\right]\mathrm{d}x\\
&+\frac{1}{2}\sum_{i=3,5,\ldots}^{2N-1}\int_0^{l_b}\left[\begin{array}{c}S_{vz_{(i,i+1)}}(\mathcal{W}_i^R-\mathcal{W}_{i+1}^R)^2+S_{vz_{(i,i+2)}}(\mathcal{W}_i^R-\mathcal{W}_{i+2}^R)^2(1-\delta_{(2N-1)(i)})\\
+S_{vz_{(i,i+3)}}(\mathcal{W}_i^R-\mathcal{W}_{i+3}^R)^2(1-\delta_{(2N-1)(i)})+S_{vz_{(i,i-2)}}(\mathcal{W}_i^R-\mathcal{W}_{i-2}^R)^2\\
(1-\delta_{1i})+S_{vz_{(i,i-1)}}(\mathcal{W}_i^R-\mathcal{W}_{i-1}^R)^2(1-\delta_{1i})\end{array}\right]\mathrm{d}x,\end{aligned} \tag{9}$$

where δ_{ij}, $(M_{bz_i}^{nl})^R$, and $(M_{by_i}^{nl})^R$ denote Kronecker delta tensor, flexural moments in the nonlocal form using the Rayleigh beam theory. Further, E_{b_i} is the elastic modulus, and N denotes the total number of constitutive DWCNTs of the membrane. The bidirectional flexural moments can be linked to their corresponding local expressions by [62, 63]:

$$(M_{by_i}^{nl})^R-l_s^2\frac{\partial^2(M_{by_i}^{nl})^R}{\partial x^2}=-E_{b_i}I_{b_i}\frac{\partial^2 \mathcal{W}_i^R}{\partial x^2}, \tag{10a}$$

$$(M_{bz_i}^{nl})^R-l_s^2\frac{\partial^2(M_{bz_i}^{nl})^R}{\partial x^2}=-E_{b_i}I_{b_i}\frac{\partial^2 \mathcal{V}_i^R}{\partial x^2}, \tag{10b}$$

in which l_s is the small-scale factor. By utilizing the principle of Hamilton and exploiting equations (9) and (8) the nonlocal-dimensionless governing equations that display lateral motion of vertically aligned single-layered membranes of DWCNTs confined by an elastic medium according to the NRBM are gained:

• The first DWCNTs:

$$\overline{\Lambda}\left\{\begin{array}{l}(\varrho_1^2\delta_{j2}+\delta_{j1})\dfrac{\partial^2\overline{\mathcal{V}}_j^R}{\partial\tau^2}-\left(\dfrac{\varrho_2^2\delta_{j2}+\delta_{j1}}{\lambda_1^2}\right)\dfrac{\partial^4\overline{\mathcal{V}}_j^R}{\partial\tau^2\partial\xi^2}+\overline{S}^R_{vy_{(j,3-j)}}(\overline{\mathcal{V}}_j^R-\overline{\mathcal{V}}_{3-j}^R)+\\ \overline{S}^R_{vy_{(j,3)}}(\overline{\mathcal{V}}_j^R-\overline{\mathcal{V}}_3^R)+\overline{S}^R_{vy_{(j,4)}}(\overline{\mathcal{V}}_j^R-\overline{\mathcal{V}}_4^R)+\left(\overline{K}_t^R\overline{\mathcal{V}}_j^R-\overline{K}_r^R\dfrac{\partial^2\overline{\mathcal{V}}_j^R}{\partial\xi^2}\right)(1-\delta_{j1})\end{array}\right\}$$
$$+(\varrho_3^2\delta_{j2}+\delta_{j1})\frac{\partial^4\bar{\mathcal{V}}_j^R}{\partial\xi^4}=0, \tag{11a}$$

$$\overline{\Lambda}\left\{\begin{array}{l}(\varrho_1^2\delta_{j2}+\delta_{j1})\dfrac{\partial^2\overline{\mathcal{W}}_j^R}{\partial\tau^2}-\dfrac{(\varrho_2^2\delta_{j2}+\delta_{j1})}{\lambda_1^2}\dfrac{\partial^4\overline{\mathcal{W}}_j^R}{\partial\tau^2\partial\xi^2}+\overline{S}^R_{vz_{(j,3-j)}}(\overline{\mathcal{W}}_j^R-\overline{\mathcal{W}}_{3-j}^R)+\\ \overline{S}^R_{vz_{(j,3)}}(\overline{\mathcal{W}}_j^R-\overline{\mathcal{W}}_3^R)+\overline{S}^R_{vz_{(j,4)}}(\overline{\mathcal{W}}_j^R-\overline{\mathcal{W}}_4^R)+\left(\overline{K}_t^R\overline{\mathcal{W}}_j^R-\overline{K}_r^R\dfrac{\partial^2\overline{\mathcal{W}}_j^R}{\partial\xi^2}\right)(1-\delta_{j1})\end{array}\right\}$$
$$+(\varrho_3^2\delta_{j2}+\delta_{j1})\frac{\partial^4\bar{\mathcal{W}}_j^R}{\partial\xi^4}=0. \tag{11b}$$

• The intermediate DWCNTs:

$$\overline{\Lambda}\left\{\begin{array}{l}(\varrho_1^2\delta_{j2}+\delta_{j1})\dfrac{\partial^2\overline{\mathcal{V}}^R_{2n-2+j}}{\partial\tau^2}-\left(\dfrac{\varrho_2^2\delta_{j2}+\delta_{j1}}{\lambda_1^2}\right)\dfrac{\partial^4\overline{\mathcal{V}}^R_{2n-2+j}}{\partial\tau^2\partial\xi^2}+\overline{S}^R_{vy_{(2n-2+j,2n+1-j)}}\times\\ (\overline{\mathcal{V}}^R_{2n-2+j}-\overline{\mathcal{V}}^R_{2n+1-j})+\overline{S}^R_{vy_{(2n-2+j,2n-2)}}(\overline{\mathcal{V}}^R_{2n-2+j}-\overline{\mathcal{V}}^R_{2n-2})+\overline{S}^R_{vy_{(2n-2+j,2n-3)}}\times\\ (\overline{\mathcal{V}}^R_{2n-2+j}-\overline{\mathcal{V}}^R_{2n-3})+\overline{S}^R_{vy_{(2n-2+j,2n+1)}}(\overline{\mathcal{V}}^R_{2n-2+j}-\overline{\mathcal{V}}^R_{2n+1})+\overline{S}^R_{vy_{(2n-2+j,2n+2)}}\times\\ (\overline{\mathcal{V}}^R_{2n-2+j}-\overline{\mathcal{V}}^R_{2n-3})+\left(\overline{K}_t^R\overline{\mathcal{V}}^R_{2n-2+j}-\overline{K}_r^R\dfrac{\partial^2\overline{\mathcal{V}}^R_{2n-2+j}}{\partial\xi^2}\right)(1-\delta_{j1})\end{array}\right\}$$
$$+(\varrho_3^2\delta_{j2}+\delta_{j1})\frac{\partial^4\overline{\mathcal{V}}^R_{2n-2+j}}{\partial\xi^4}=0, \tag{12a}$$

$$\overline{\Lambda}\left\{\begin{array}{l}(\varrho_1^2\delta_{j2}+\delta_{j1})\dfrac{\partial^2\overline{\mathcal{W}}^R_{(2n-2+j)}}{\partial\tau^2}-\left(\dfrac{\varrho_2^2\delta_{j2}+\delta_{j1}}{\lambda_1^2}\right)\dfrac{\partial^4\overline{\mathcal{W}}^R_{2n-2+j}}{\partial\tau^2\partial\xi^2}+\overline{S}^R_{vz_{(2n-2+j,2n+1-j)}}\times\\ (\overline{\mathcal{W}}^R_{2n-2+j}-\overline{\mathcal{W}}^R_{2n+1-j})+\overline{S}^R_{vz_{(2n-2+j,2n-2)}}(\overline{\mathcal{W}}^R_{2n-2+j}-\overline{\mathcal{W}}^R_{2n-2})+\overline{S}^R_{vz_{(2n-2+j,2n-3)}}\times\\ (\overline{\mathcal{W}}^R_{2n-2+j}-\overline{\mathcal{W}}^R_{2n-3})+\overline{S}^R_{vz_{(2n-2+j,2n+1)}}(\overline{\mathcal{W}}^R_{2n-2+j}-\overline{\mathcal{W}}^R_{2n+1})+\overline{S}^R_{vz_{(2n-2+j,2n+2)}}\times\\ (\overline{\mathcal{W}}^R_{2n-2+j}-\overline{\mathcal{W}}^R_{2n+2})+\left(\overline{K}_t^R\overline{\mathcal{W}}^R_{2n-2+j}-\overline{K}_r^R\dfrac{\partial^2\overline{\mathcal{W}}^R_{2n-2+j}}{\partial\xi^2}\right)(1-\delta_{j1})\end{array}\right\}$$
$$+(\varrho_3^2\delta_{j2}+\delta_{j1})\frac{\partial^4\overline{\mathcal{W}}^R_{2n-2+j}}{\partial\xi^4}=0. \tag{12b}$$

• The *N*th DWCNTs:

$$\overline{\Lambda}\left\{\begin{array}{c}(\varrho_1^2\delta_{j2}+\delta_{j1})\dfrac{\partial^2\overline{\mathcal{V}}^R_{2N-2+j}}{\partial\tau^2}-\left(\dfrac{\varrho_2^2\delta_{j2}+\delta_{j1}}{\lambda_1^2}\right)\dfrac{\partial^4\overline{\mathcal{V}}^R_{2N-2+j}}{\partial\tau^2\partial\xi^2}+\overline{S}^R_{vy_{(2N-2+j,2N+1-j)}}\times\\ (\overline{\mathcal{V}}^R_{2N-2+j}-\overline{\mathcal{V}}^R_{2N+1-j})+\overline{S}^R_{vy_{(2N-2+j,2-2)}}(\overline{\mathcal{V}}^R_{2N-2+j}-\overline{\mathcal{V}}^R_{2N-2})\\ +\overline{S}^R_{vy_{(2N-2+j,2-3)}}(\overline{\mathcal{V}}^R_{2N-2+j}-\overline{\mathcal{V}}^R_{2N-3})+\left(\overline{K}_t^R\overline{\mathcal{V}}^R_{2N-2+j}-\overline{K}_r^R\dfrac{\partial^2\overline{\mathcal{V}}^R_{2N-2+j}}{\partial\xi^2}\right)(1-\delta_{j1})\end{array}\right\}$$
$$+(\varrho_3^2\delta_{j2}+\delta_{j1})\frac{\partial^4\overline{\mathcal{V}}^R_{2N-2+j}}{\partial\xi^4}=0, \tag{13a}$$

$$\overline{\Lambda}\left\{\begin{array}{c}(\varrho_1^2\delta_{j2}+\delta_{j1})\dfrac{\partial^2\overline{\mathcal{W}}^R_{2N-2+j}}{\partial\tau^2}-\left(\dfrac{\varrho_2^2\delta_{j2}+\delta_{j1}}{\lambda_1^2}\right)\dfrac{\partial^4\overline{\mathcal{W}}^R_{2N-2+j}}{\partial\tau^2\partial\xi^2}+\overline{S}^R_{vz_{(2N-2+j,2N+1-j)}}\times\\ (\overline{\mathcal{W}}^R_{2N-2+j}-\overline{\mathcal{W}}^R_{2N+1-j})+\overline{S}^R_{vz_{(2N-2+j,2-2)}}(\overline{\mathcal{W}}^R_{2N-2+j}-\overline{\mathcal{W}}^R_{2N-2})\\ +\overline{S}^R_{vz_{(2N-2+j,2-3)}}(\overline{\mathcal{W}}^R_{2N-2+j}-\overline{\mathcal{W}}^R_{2N-3})+\left(\overline{K}_t^R\overline{\mathcal{W}}^R_{2N-2+j}-\overline{K}_r^R\dfrac{\partial^2\overline{\mathcal{W}}^R_{2N-2+j}}{\partial\xi^2}\right)(1-\delta_{j1})\end{array}\right\}$$
$$+(\varrho_3^2\delta_{j2}+\delta_{j1})\frac{\partial^4\overline{\mathcal{W}}^R_{2N-2+j}}{\partial\xi^4}=0. \tag{13b}$$

In these dimensionless equations, $j=1$ and $j=2$ stand for the innermost and outermost tubes, respectively, $\overline{\Lambda}[\cdot]=[\cdot]-\mu^2\frac{\partial^2}{\partial\xi^2}[\cdot]$ represents the dimensionless nonlocal operator, and other dimensionless quantities are as:

$$\xi=\frac{x}{l_b},\ \gamma=\frac{z}{l_z},\ \overline{\mathcal{V}}_i^R=\frac{\mathcal{V}_i^R}{l_b},\ \overline{\mathcal{W}}_i^R=\frac{\mathcal{W}_i^R}{l_b},\ \tau=\frac{t}{l_b^2}\sqrt{\frac{E_{b_1}I_{b_1}}{\rho_{b_1}A_{b_1}}},\ \mu=\frac{l_s}{l_b},$$
$$\varrho_1^2=\frac{\rho_{b_2}A_{b_2}}{\rho_{b_1}A_{b_1}},\ \varrho_2^2=\frac{\rho_{b_2}I_{b_2}}{\rho_{b_1}I_{b_1}},\ \varrho_3^2=\frac{E_{b_2}I_{b_2}}{E_{b_1}I_{b_1}},\ \overline{K}_t^R=\frac{K_tl_b^4}{E_{b_1}I_{b_1}},\ \overline{K}_r^R=\frac{K_rl_b^2}{E_{b_1}I_{b_1}},$$
$$\overline{S}^R_{vy_{(m,n)}}=\frac{S_{vy_{(m,n)}}l_b^4}{E_{b_1}I_{b_1}},\ \overline{S}^R_{vz_{(m,n)}}=\frac{S_{vz_{(m,n)}}l_b^4}{E_{b_1}I_{b_1}},\ l_z=(N-1)d,\ \lambda_1=\frac{l_b}{\sqrt{\frac{I_{b_1}}{A_{b_1}}}}. \tag{14}$$

Equations (11)–(13) display $4N$ coupled partial differential equations of fourth-order with respect to the spatial parameter. For lowly dense membranes made from DWCNTs, these equations could be easily used for examining their lateral vibrations. Nevertheless, the number of governing equations drastically increases as the number of the constitutive DWCNTs grows. This crucial issue motivates the authors to seek for more appropriate models whose equations can be presented in a more compact form. The details of these calculations will be presented in section 3.

2.2.2. Determination of the natural frequencies. In this section, the assumed mode method (AMM) is implemented for analyzing of the free dynamic response of the vertically aligned confined single-layered membranes of DWCNTs. For this purpose, the ended supports of all consisting tubes are assumed to be simple such that the outside nanotubes of both 1st and *N*th DWCNTs are laterally fixed. By exploiting the AMM, the deflections of the consisting nanotubes can be displayed by:

$$\langle\overline{\mathcal{V}}_i^R(\xi,\tau),\overline{\mathcal{W}}_i^R(\xi,\tau)\rangle=\left\langle\sum_{m=1}^{M_{my}}\overline{v}_{im}^R(\tau)\sin(m\pi\xi),\sum_{m=1}^{M_{mz}}\overline{\mathcal{W}}_{im}^R(\tau)\sin(m\pi\xi)\right\rangle, \tag{15}$$

where $\overline{v}_{im}^R(\tau)$ and $\overline{\mathcal{W}}_{im}^R(\tau)$ are the coefficients of the *m*th mode of the *i*th tube, M_{my} and M_{mz} are the total number of vibrational modes exploited for discretization of the deflections $\overline{\mathcal{V}}_i^R(\xi,\tau)$ and $\overline{\mathcal{W}}_i^R(\xi,\tau)$, respectively. By substituting equation (15) into equations (11)–(13),

$$\frac{\mathrm{d}^2\overline{\mathbf{x}}^R}{\mathrm{d}\tau^2}+\overline{\mathbf{\Gamma}}^R\overline{\mathbf{x}}^R=0, \tag{16}$$

in which $\overline{\mathbf{x}}^R$ is the vector of the dimensionless time-dependent factors such that:

$$\overline{\mathbf{x}}^R = \{[.]^R_{1m}, [.]^R_{3m}, [.]^R_{4m}, [.]^R_{5m} \ \cdots \ [.]^R_{(2N-2)m}, [.]^R_{(2N-1)m}\}^T,$$
$$[.] = V \ or \ W, \tag{17}$$

and the non-vanishing elements of the square matrix $\overline{\mathbf{\Gamma}}^R$ are provided in the supplementary material available online at stacks.iop.org/PS/95/035221/mmedia, part A. Now by substituting $\overline{\mathbf{x}}^R = \overline{\mathbf{x}}^R_0 \exp(\mathrm{i}\varpi^R\tau)$ into equation (16), the flexural frequencies in the dimensionless manner can be computed through finding the roots of the following characteristic relation: $|-(\varpi^R)^2\,\delta_{ij} + \overline{\mathbf{\Gamma}}^R_{ij}| = 0$, where $\overline{\mathbf{x}}^R_0$ and ϖ^R in order represent the dimensionless amplitude vector and the dimensionless frequency of the NRBM-based nanosystem, respectively. Finally, the ith natural frequency can be evaluated from: $\omega^R_i = \frac{\varpi^R_i}{l_b^2}\sqrt{\frac{E_{b_1}I_{b_1}}{\rho_{b_1}A_{b_1}}}$.

2.3. Application of the NTBM for discrete modeling of membranes of DWCNTs

2.3.1. Nonlocal-discrete equations of motion. For an elastically embedded nanosystem consists of N vertically aligned DWCNTs, its whole kinetic energy according to the Timoshenko beam model is written as:

$$T^T(t) = \frac{1}{2}\sum_{i=1}^{2N}\int_0^{l_b}\rho_{b_i}\left(A_{b_i}\left(\left(\frac{\partial \mathcal{V}_i^T}{\partial t}\right)^2 + \left(\frac{\partial \mathcal{W}_i^T}{\partial t}\right)^2\right) + I_{b_i}\left(\left(\frac{\partial \Theta^T_{z_i}}{\partial t}\right)^2 + \left(\frac{\partial \Theta^T_{y_i}}{\partial t}\right)^2\right)\right)\mathrm{d}x, \tag{18}$$

where $\mathcal{V}_i^T$ and $\mathcal{W}_i^T$ in order are the y- and z-directional components of the deflection vector field of the ith tube, Θ^T_{yi} and Θ^T_{zi} denote their corresponding deflections' angles.

Additionally, the whole nonlocal strain energy of the elastically confined single-layered DWCNTs whose tubes have been modeled based on the Timoshenko beam model can be evaluated as follows:

$$\begin{aligned}
U^T(t) = {} & \frac{1}{2}\sum_{i=1}^{2N} \times \int_0^{l_b}\begin{bmatrix} -\dfrac{\partial \Theta^T_{z_i}}{\partial x}(M^{nl}_{bz_i})^T + \left(\dfrac{\partial V_i^T}{\partial x} - \Theta^T_{z_i}\right)(Q^{nl}_{by_i})^T \\ -\dfrac{\partial \Theta^T_{yi}}{\partial x}(M^{nl}_{by_i})^T + \left(\dfrac{\partial W_i^T}{\partial x} - \Theta^T_{y_i}\right)(Q^{nl}_{by_i})^T \end{bmatrix}\mathrm{d}x \\
& + \frac{1}{2}\sum_{i=2,4,\ldots}^{2N}\int_0^{l_b}\begin{bmatrix} S_{vy_{(i,i-1)}}(V_i^T - V_{i-1}^T)^2 + S_{vy_{(i,i+2)}}(V_i^T - V_{i+2}^T)^2(1-\delta_{(2N)(i)}) \\ +S_{vy_{(i,i+1)}}(V_i^T - V_{i+1}^T)^2(1-\delta_{(2N)(i)}) + S_{vy_{(i,i-2)}}(V_i^T - V_{i-2}^T)^2(1-\delta_{2i}) \\ +S_{vy_{(i,i-3)}}(V_i^T - V_{i-3}^T)^2(1-\delta_{2i}) + K_t(V_i^T)^2 + K_r(\Theta^T_{z_i})^2 \end{bmatrix}\mathrm{d}x \\
& + \frac{1}{2}\sum_{i=3,5\ldots}^{2N-1}\int_0^{l_b}\begin{bmatrix} S_{vy_{(i,i+1)}}(V_i^T - V_{i+1}^T)^2 + S_{vy_{(i,i+2)}}(V_i^T - V_{i+2}^T)^2(1-\delta_{(2N-1)(i)}) + \\ S_{vy_{(i,i+3)}}(V_i^T - V_{i+3}^T)^2(1-\delta_{(2N-1)(i)}) + S_{vy_{(i,i-2)}}(V_i^T - V_{i-2}^T)^2(1-\delta_{1i}) \\ +S_{vy_{(i,i-1)}}(V_i^T - V_{i-1}^T)^2(1-\delta_{1i}) \end{bmatrix}\mathrm{d}x \\
& + \frac{1}{2}\sum_{i=2,4,\ldots}^{2N}\int_0^{l_b}\begin{bmatrix} S_{vz_{(i,i-1)}}(W_i^T - W_{i-1}^T)^2 + S_{vz_{(i,i+2)}}(W_i^T - W_{i+2}^T)^2(1-\delta_{(2N)(i)}) \\ +S_{vz_{(i,i+1)}}(W_i^T - W_{i+1}^T)^2(1-\delta_{(2N)(i)}) + \\ S_{vz_{(i,i-2)}}(W_i^T - W_{i-2}^T)^2(1-\delta_{2i}) + S_{vz_{(i,i-3)}}(W_i^T - W_{i-3}^T)^2(1-\delta_{2i}) + \\ K_t(W_i^T)^2 + K_r(\Theta^T_{y_j})^2 \end{bmatrix}\mathrm{d}x \\
& + \frac{1}{2}\sum_{i=3,5,\ldots}^{2N-1}\int_0^{l_b}\begin{bmatrix} S_{vz_{(i,i+1)}}(W_i^T - W_{i+1}^T)^2 + S_{vz_{(i,i+2)}}(W_i^T - W_{i+2}^T)^2(1-\delta_{(2N-1)(i)}) \\ +S_{vz_{(i,i+3)}}(W_i^T - W_{i+3}^T)^2(1-\delta_{(2N-1)(i)}) + S_{vz_{(i,i-2)}}(W_i^T - W_{i-2}^T)^2 \\ (1-\delta_{1i}) + S_{vz_{(i,i-1)}}(W_i^T - W_{i-1}^T)^2(1-\delta_{1i}) \end{bmatrix}\mathrm{d}x,
\end{aligned} \tag{19}$$

where $(Q_{by_i}^{nl})^T$ and $(Q_{bz_i}^{nl})^T$ in order represent the components of the resultant shear force of the ith continuum-based tube, $(M_{bz_i}^{nl})^T$ and $(M_{by_i}^{nl})^T$ denote the components of the flexural moment in the context of the NTBM. On the basis of the Eringen's nonlocal continuum mechanics, these nonlocal forces can be linked to their associated local values by the following constitutive relations [64, 65]:

$$(Q_{by_i}^{nl})^T - l_s^2 \frac{\partial^2 (Q_{by_i}^{nl})^T}{\partial x^2} = k_{s_i} G_{b_i} A_{b_i} \left(\frac{\partial \mathcal{V}_i^T}{\partial x} - \Theta_{z_i}^T \right), \tag{20a}$$

$$(Q_{bz_i}^{nl})^T - l_s^2 \frac{\partial^2 (Q_{bz_i}^{nl})^T}{\partial x^2} = k_{s_i} G_{b_i} A_{b_i} \left(\frac{\partial \mathcal{W}_i^T}{\partial x} - \Theta_{y_i}^T \right), \tag{20b}$$

$$(M_{by_i}^{nl})^T - l_s^2 \frac{\partial^2 (M_{by_i}^{nl})^T}{\partial x^2} = -E_{b_i} I_{b_i} \frac{\partial \Theta_{y_i}^T}{\partial x}, \tag{20c}$$

$$(M_{bz_i}^{nl})^T - l_s^2 \frac{\partial^2 (M_{bz_i}^{nl})^T}{\partial x^2} = -E_{b_i} I_{b_i} \frac{\partial \Theta_{z_i}^T}{\partial x}, \tag{20d}$$

where G_{b_i} and k_{s_i} in order are the shear elastic modulus of the ECS and the shear correction factor of the ith continuum-based nanotube.

By adopting the principle of Hamilton, in view of equations (18), (19), (20*a*)–(20*d*), the nonlocal-dimensionless equations that display bidirectional lateral motions of the elastically confined nanoscaled system via the NTBM are resulted in as:

- The first DWCNTs:

$$\bar{\Lambda}\left\{ \frac{(\varrho_2^2 \delta_{j2} + \delta_{j1})}{\lambda_1^2} \frac{\partial^2 \overline{\Theta}_{z_j}^T}{\partial \tau^2} + \overline{K}_r^T \overline{\Theta}_{z_j}^T (1 - \delta_{j1}) \right\} - (\varrho_4^2 \delta_{j2} + \delta_{j1}) \left(\frac{\partial \overline{\mathcal{V}}_j^T}{\partial \xi} - \overline{\Theta}_{z_j}^T \right) - (\varrho_3^2 \delta_{j2} + \delta_{j1}) \eta \frac{\partial^2 \overline{\Theta}_{z_j}^T}{\partial \xi^2} = 0, \tag{21a}$$

$$\overline{\Lambda}\left\{ \begin{array}{c} (\varrho_1^2 \delta_{j2} + \delta_{j1}) \frac{\partial^2 \overline{\mathcal{V}}_j^T}{\partial \tau^2} + \overline{S}_{vy_{(j,3-j)}}^T (\overline{\mathcal{V}}_j^T - \overline{\mathcal{V}}_{3-j}^T) + \overline{S}_{vy_{(j,3)}}^T (\overline{\mathcal{V}}_j^T - \overline{\mathcal{V}}_3^T) \\ + \overline{S}_{vy_{(j,4)}}^T (\overline{\mathcal{V}}_j^T - \overline{\mathcal{V}}_4^T) + \overline{K}_t^T \overline{\mathcal{V}}_j^T (1 - \delta_{j1}) \end{array} \right\} - (\varrho_4^2 \delta_{j2} + \delta_{j1}) \left(\frac{\partial^2 \overline{\mathcal{V}}_j^T}{\partial \xi^2} - \frac{\partial \overline{\Theta}_{z_j}^T}{\partial \xi} \right) = 0, \tag{21b}$$

$$\bar{\Lambda}\left\{ \frac{(\varrho_2^2 \delta_{j2} + \delta_{j1})}{\lambda_1^2} \frac{\partial^2 \overline{\Theta}_{y_j}^T}{\partial \tau^2} + \overline{K}_r^T \overline{\Theta}_{y_j}^T (1 - \delta_{j1}) \right\} - (\varrho_4^2 \delta_{j2} + \delta_{j1}) \left(\frac{\partial \overline{\mathcal{W}}_j^T}{\partial \xi} - \overline{\Theta}_{y_j}^T \right) - (\varrho_3^2 \delta_{j2} + \delta_{j1}) \eta \frac{\partial^2 \overline{\Theta}_{y_j}^T}{\partial \xi^2} = 0, \tag{21c}$$

$$\overline{\Lambda}\left\{ \begin{array}{c} (\varrho_1^2 \delta_{j2} + \delta_{j1}) \frac{\partial^2 \overline{\mathcal{W}}_j^T}{\partial \tau^2} + \overline{S}_{vz_{(j,3-j)}}^T (\overline{\mathcal{W}}_j^T - \overline{\mathcal{W}}_{3-j}^T) + \overline{S}_{vz_{(j,3)}}^T (\overline{\mathcal{W}}_j^T - \overline{\mathcal{W}}_3^T) \\ + \overline{S}_{vz_{(j,4)}}^T (\overline{\mathcal{W}}_j^T - \overline{\mathcal{W}}_4^T) + \overline{K}_t^T \overline{\mathcal{V}}_j^T (1 - \delta_{j1}) \end{array} \right\} - (\varrho_4^2 \delta_{j2} + \delta_{j1}) \left(\frac{\partial^2 \overline{\mathcal{W}}_j^T}{\partial \xi^2} - \frac{\partial \overline{\Theta}_{y_j}^T}{\partial \xi} \right) = 0. \tag{21d}$$

- The intermediate DWCNTs:

$$\begin{aligned} &\bar{\Lambda}\left\{ \frac{(\varrho_2^2 \delta_{j2} + \delta_{j1})}{\lambda_1^2} \frac{\partial^2 \overline{\Theta}_{z_{2n-2+j}}^T}{\partial \tau^2} + \overline{K}_r^T \overline{\Theta}_{z_{2n-2+j}}^T (1 - \delta_{j1}) \right\} - (\varrho_4^2 \delta_{j2} + \delta_{j1}) \\ &\times \left(\frac{\partial \overline{\mathcal{V}}_{(2n-2+j)}^T}{\partial \xi} - \overline{\Theta}_{z_{2n-2+j}}^T \right) - (\varrho_3^2 \delta_{j2} + \delta_{j1}) \eta \frac{\partial^2 \overline{\Theta}_{z_{2n-2+j}}^T}{\partial \xi^2} = 0, \end{aligned} \tag{22a}$$

$$\overline{\Lambda}\left\{\begin{array}{c}(\varrho_1^2\delta_{j2}+\delta_{j1})\frac{\partial^2\overline{\mathcal{V}}^T_{2n-2+j}}{\partial\tau^2}+\overline{S}^T_{vy_{(2n-2+j,2n+1-j)}}(\overline{\mathcal{V}}^T_{2n-2+j}-\overline{\mathcal{V}}^T_{2n+1-j})+\\ \overline{S}^T_{vy_{(2n-2+j,2n-2)}}(\overline{\mathcal{V}}^T_{2n-2+j}-\overline{\mathcal{V}}^T_{2n-2})+\overline{S}^T_{vy_{(2n-2+j,2n-3)}}(\overline{\mathcal{V}}^T_{2n-2+j}-\overline{\mathcal{V}}^T_{2n-3})+\\ \overline{S}^T_{vy_{(2n-2+j,2n+1)}}(\overline{\mathcal{V}}^T_{2n-2+j}-\overline{\mathcal{V}}^T_{2n+1})+\overline{S}^T_{vy_{(2n-2+j,2n+2)}}(\overline{\mathcal{V}}^T_{2n-2+j}-\overline{\mathcal{V}}^T_{2n+2})+\\ \overline{K}_t^T\overline{\mathcal{V}}^T_{2n-2+j}(1-\delta_{j1})\end{array}\right\}$$
$$-(\varrho_4^2\delta_{j2}+\delta_{j1})\left(\frac{\partial^2\overline{\mathcal{V}}^T_{2n-2+j}}{\partial\xi^2}-\frac{\partial\overline{\Theta}^T_{z_{2n-2+j}}}{\partial\xi}\right)=0, \tag{22b}$$

$$\bar{\Lambda}\left\{\frac{(\varrho_2^2\delta_{j2}+\delta_{j1})}{\lambda_1^2}\frac{\partial^2\overline{\Theta}^T_{y_{2n-2+j}}}{\partial\tau^2}+\overline{K}_r^T\overline{\Theta}^T_{y_{2n-2+j}}(1-\delta_{j1})\right\}-(\varrho_4^2\delta_{j2}+\delta_{j1})$$
$$\times\left(\frac{\partial\overline{\mathcal{W}}^T_{(2n-2+j)}}{\partial\xi}-\overline{\Theta}^T_{y_{2n-2+j}}\right)-(\varrho_3^2\delta_{j2}+\delta_{j1})\eta\frac{\partial^2\overline{\Theta}^T_{y_{2n-2+j}}}{\partial\xi^2}=0, \tag{22c}$$

$$\overline{\Lambda}\left\{\begin{array}{c}(\varrho_1^2\delta_{j2}+\delta_{j1})\frac{\partial^2\overline{\mathcal{W}}^T_{(2n-2+j)}}{\partial\tau^2}+\overline{S}^T_{vz_{(2n-2+j,2n+1-j)}}(\overline{\mathcal{W}}^T_{2n-2+j}-\overline{\mathcal{W}}^T_{2n+1-j})+\\ \overline{S}^T_{vz_{(2n-2+j,2n-2)}}(\overline{\mathcal{W}}^T_{2n-2+j}-\overline{\mathcal{W}}^T_{(2n-2)})+\overline{S}^T_{vz_{(2n-2+j,2n-3)}}(\overline{\mathcal{W}}^T_{2n-2+j}-\overline{\mathcal{W}}^T_{2n-3})+\\ \overline{S}^T_{vz_{(2n-2+j,2n+1)}}(\overline{\mathcal{W}}^T_{2n-2+j}-\overline{\mathcal{W}}^T_{2n+1})+\overline{S}^T_{vz_{(2n-2+j,2n+2)}}(\overline{\mathcal{W}}^T_{2n-2+j}-\overline{\mathcal{W}}^T_{2n+2})+\\ \overline{K}_t^T\overline{\mathcal{W}}^T_{2n-2+j}(1-\delta_{j1})\end{array}\right\}$$
$$-(\varrho_4^2\delta_{j2}+\delta_{j1})\left(\frac{\partial^2\overline{\mathcal{W}}^T_{2n-2+j}}{\partial\xi^2}-\frac{\partial\overline{\Theta}^T_{y_{2n-2+j}}}{\partial\xi}\right)=0. \tag{22d}$$

• The *N*th DWCNTs:

$$\bar{\Lambda}\left\{\frac{(\varrho_2^2\delta_{j2}+\delta_{j1})}{\lambda_1^2}\frac{\partial^2\overline{\Theta}^T_{z_{2N-2+j}}}{\partial\tau^2}+\overline{K}_r^T\overline{\Theta}^T_{z_{2N-2+j}}(1-\delta_{j1})\right\}-(\varrho_4^2\delta_{j2}+\delta_{j1})$$
$$\times\left(\frac{\partial\overline{\mathcal{V}}^T_{(2N-2+j)}}{\partial\xi}-\overline{\Theta}^T_{z_{2N-2+j}}\right)-(\varrho_3^2\delta_{j2}+\delta_{j1})\eta\frac{\partial^2\overline{\Theta}^T_{z_{2N-2+j}}}{\partial\xi^2}=0, \tag{23a}$$

$$\overline{\Lambda}\left\{\begin{array}{c}(\varrho_1^2\delta_{j2}+\delta_{j1})\frac{\partial^2\overline{\mathcal{V}}^T_{2N-2+j}}{\partial\tau^2}+\overline{S}^T_{vy_{(2N-2+j,2N+1-j)}}(\overline{\mathcal{V}}^T_{2N-2+j}-\overline{\mathcal{V}}^T_{2N+1-j})\\ +\overline{S}^T_{vy_{(2N-2+j,2-2)}}(\overline{\mathcal{V}}^T_{2N-2+j}-\overline{\mathcal{V}}^T_{2N-2})+\overline{S}^T_{vy_{(2N-2+j,2-3)}}(\overline{\mathcal{V}}^T_{2N-2+j}-\overline{\mathcal{V}}^T_{2N-3})\\ +\overline{K}_t^T\overline{\mathcal{V}}^T_{2N-2+j}(1-\delta_{j1})\end{array}\right\}-(\varrho_4^2\delta_{j2}+\delta_{j1})\left(\frac{\partial^2\overline{\mathcal{V}}^T_{2N-2+j}}{\partial\xi^2}-\frac{\partial\overline{\Theta}^T_{z_{2N-2+j}}}{\partial\xi}\right)=0, \tag{23b}$$

$$\bar{\Lambda}\left\{\frac{(\varrho_2^2\delta_{j2}+\delta_{j1})}{\lambda_1^2}\frac{\partial^2\overline{\Theta}^T_{y_{2N-2+j}}}{\partial\tau^2}+\overline{K}_r^T\overline{\Theta}^T_{y_{2N-2+j}}(1-\delta_{j1})\right\}-(\varrho_4^2\delta_{j2}+\delta_{j1})$$
$$\times\left(\frac{\partial\overline{\mathcal{W}}^T_{(2N-2+j)}}{\partial\xi}-\overline{\Theta}^T_{y_{2N-2+j}}\right)-(\varrho_3^2\delta_{j2}+\delta_{j1})\eta\frac{\partial^2\overline{\Theta}^T_{y_{2N-2+j}}}{\partial\xi^2}=0, \tag{23c}$$

$$\overline{\Lambda}\left\{\begin{array}{c}(\varrho_1^2\delta_{j2}+\delta_{j1})\frac{\partial^2\overline{\mathcal{W}}^T_{(2N-2+j)}}{\partial\tau^2}+\overline{S}^T_{vz_{(2N-2+j,2N+1-j)}}(\overline{\mathcal{W}}^T_{2N-2+j}-\overline{\mathcal{W}}^T_{2N+1-j})\\ +\overline{S}^T_{vz_{(2N-2+j,2-2)}}(\overline{\mathcal{W}}^T_{2N-2+j}-\overline{\mathcal{W}}^T_{2N-2})+\overline{S}^T_{vz_{(2N-2+j,2-3)}}(\overline{\mathcal{W}}^T_{2N-2+j}-\overline{\mathcal{W}}^T_{2N-3})\\ +\overline{K}_t^T\overline{\mathcal{W}}^T_{2N-2+j}(1-\delta_{j1})\end{array}\right\}$$
$$-(\varrho_4^2\delta_{j2}+\delta_{j1})\left(\frac{\partial^2\overline{\mathcal{W}}^T_{2N-2+j}}{\partial\xi^2}-\frac{\partial\overline{\Theta}^T_{y_{2N-2+j}}}{\partial\xi}\right)=0, \tag{23d}$$

where the newly used dimensionless parameters are as follows:

$$\begin{aligned}\overline{\mathcal{V}}_i^T &= \frac{\mathcal{V}_i^T}{l_b},\ \overline{\mathcal{W}}_i^T=\frac{\mathcal{W}_i^T}{l_b},\ \tau=\frac{t}{l_b}\sqrt{\frac{k_{s_1}G_{b_1}}{\rho_{b_1}}},\ \overline{S}^T_{vy_{(m,n)}} = \frac{S_{vy_{(m,n)}}l_b^2}{k_{s_1}G_{b_1}A_{b_1}},\ \overline{S}^T_{vz_{(m,n)}}=\frac{S_{vz_{(m,n)}}l_b^2}{k_{s_1}G_{b_1}A_{b_1}},\\ \varrho_4^2 &= \frac{k_{s2}G_{b2}A_{b2}}{k_{s1}G_{b1}A_{b1}},\ \overline{\Theta}^T_{y_i}=\Theta^T_{y_i},\ \overline{\Theta}^T_{z_i}=\Theta^T_{z_i},\ \eta = \frac{E_{b_1}I_{b_1}}{k_{s_1}G_{b_1}A_{b_1}l_b^2},\ \overline{K}_t^T=\frac{K_tl_b^2}{k_{s_1}G_{b_1}A_{b_1}},\\ \overline{K}_r^T &= \frac{K_r}{k_{s_1}G_{b_1}A_{b_1}},\ \gamma=\frac{z}{l_z}.\end{aligned} \tag{24}$$

Equations (21)–(23) display $8N$ coupled second-order linear homogeneous partial differential equations in both time and space domains.

2.3.2. Determination of the natural frequencies. For frequency analysis of the problem at hand, it is assumed that the first and the *N*th nanotubes have been tightly attached to rigid supports. Therefore, no elastic field would be generated within such tubes during the course of free vibration. Now by implementing AMM for simply supported nanotubes, the dimensionless deformation fields of the *i*th nanotube using NTBM could be expressed by:

$$\langle\overline{\mathcal{V}}_i^T(\xi,\tau),\overline{\mathcal{W}}_i^T(\xi,\tau)\rangle = \langle\sum_{m=1}^{M_{my}}\overline{\mathcal{V}}^T_{im}(\tau)\sin(m\pi\xi),\sum_{m=1}^{M_{mz}}\overline{\mathcal{W}}^T_{im}(\tau)\sin(m\pi\xi)\rangle, \tag{25a}$$

$$\langle\overline{\Theta}^T_{z_i}(\xi,\tau),\overline{\Theta}^T_{y_i}(\xi,\tau)\rangle = \langle\sum_{m=1}^{M_{my}}\overline{\Theta}^T_{z_{im}}(\tau)\cos(m\pi\xi),\sum_{m=1}^{M_{mz}}\overline{\Theta}^T_{y_{im}}(\tau)\cos(m\pi\xi)\rangle, \tag{25b}$$

by substituting equations (25*a*) and (25*b*) into equations (23*a*)–(23*d*), it is derived:

$$\frac{\mathrm{d}^2\overline{\mathbf{x}}^T}{\mathrm{d}\tau^2}+\overline{\mathbf{\Gamma}}^T\overline{\mathbf{x}}^T=0, \tag{26}$$

in which $\overline{\mathbf{x}}^T$ (i.e. the dimensionless time-dependent vector) is defined by:

$$\overline{\mathbf{x}}^T=\{\overline{[.]}^T_{1m},\overline{[*]}^T_{1m},\overline{[.]}^T_{3m},\overline{[*]}^T_{3m},\overline{[.]}^T_{4m},\overline{[*]}^T_{4m}\ \cdots\ \overline{[.]}^T_{(2N-1)m},\overline{[*]}^T_{(2N-1)m}\}, \tag{27}$$

where $[.]=V$ or W, $[*]=\Theta_z$ or Θ_y, and the matrix $\overline{\mathbf{\Gamma}}^T$ is given in the supplementary material, part B. Let us to consider: $\overline{\mathbf{x}}^T(\tau)=\overline{\mathbf{x}}_0^T\exp(\mathrm{i}\varpi^T\tau)$ where $\overline{\mathbf{x}}_0^T$ is the amplitude vector (i.e. eigenvectors) and ϖ^T denotes the dimensionless natural frequencies of the nanosystem modeled according to the NTBM. By introducing such a harmonic form of the deformation field to equation (26), the dimensionless frequencies could be calculated from the characteristic relation: $|-(\varpi^T)^2\delta_{ij}+\overline{\mathbf{\Gamma}}^T_{ij}|=0$. Subsequently, in view of equation (24), the natural frequencies of the nanosystem can be stated as a function of their corresponding dimensionless values as follows: $\omega_i^T=\frac{\varpi_i^T}{l_b}\sqrt{\frac{k_{s_1}G_{b_1}}{\rho_{b_1}}}$.

3. Vibrational scrutiny using nonlocal continuous models

In this part we are interested in examining free transverse vibrations of elastically confined membranes from vertically aligned DWCNTs by developing nonlocal continuous models. As it was explained in the previous parts, the proposed discrete models are not capable in capturing natural frequencies of highly populated nanosystems (for a nanosystem with *N* DWCNTs, we confront to $4N$ and $8N$ set of equations based on the NRBM and NTBM). Hence, if we could express the deformation fields of the nanosystem by constructing appropriate continuous functions, the number of equations would be independent of the number of consisting tubes (i.e. we confront to 2 and 4 equations of motion in terms of the continuous deformations of the nanosystem modeled according to the NRBM and NTBM, respectively). The spatial domain of such continuous fields has been schematically illustrated in figure 3.

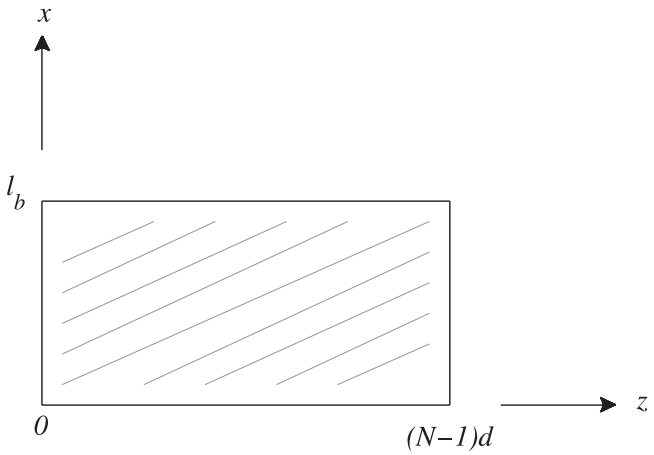

Figure 3. The side view of the spatial domain used for the continuous models.

For developing equations of motion for continuous models, we use the developed governing equations for discrete models such that the continuous displacements and the continuous deflection angles satisfy the following relations:

$$v_j^{[\cdot]}(x, z_{2n-2+j}, t) \approx \mathcal{V}_{2n-2+j}^{[\cdot]}(x, t),\ \ v_j^{[\cdot]}(x, z_{2n-4+j} - d, t) \approx \mathcal{V}_{2n-4+j}^{[\cdot]}(x, t), \tag{28a}$$

$$v_j^{[\cdot]}(x, z_{2n+j} + d, t) \approx \mathcal{V}_{2n+j}^{[\cdot]}(x, t);\ [\cdot] = R \text{ or } T, \tag{28b}$$

$$w_j^{[\cdot]}(x, z_{2n-2+j}, t) \approx \mathcal{W}_{2n-2+j}^{[\cdot]}(x, t),\ \ w_j^{[\cdot]}(x, z_{2n-4+j} - d, t) \approx \mathcal{W}_{(2n-4+j)}^{[\cdot]}(x, t), \tag{28c}$$

$$w_j^{[\cdot]}(x, z_{2n+j} + d, t) \approx \mathcal{W}_{2n+j}^{[\cdot]}(x, t), \tag{28d}$$

$$\theta_{y_j}^{T}(x, z_{2n-2+j}, t) \approx \Theta_{y_{2n-2+j}}^{T}(x, t),\ \ \theta_{z_j}^{T}(x, z_{2n-2+j}, t) \approx \Theta_{z_{2n-2+j}}^{T}(x, t). \tag{28e}$$

Thereafter, the deflections of the neighboring tubes of the mth nanotube are approximated by the following Taylor series:

$$[\circ]_j(x, z_m \pm d, t) = \sum_{i=0}^{6} \frac{(\pm d)^i}{i!} \frac{\partial^i [\circ]_j}{\partial z^i}(x, z_m, t), \tag{29}$$

where $[\circ]_j = v^{[\cdot]}$ or $w^{[\cdot]}$ and $m = 2n + j - 4$ or $2n + j$.

3.1. Application of the NRBM for continuous modeling of membranes of DWCNTs

3.1.1. Nonlocal-continuous equations of motion. By substituting equation (29) into equations (11*a*) and (11*b*) in view of equations (14), (28*a*)–(28*d*), after some manipulations, the dimensionless continuous equations of motion associated with the transverse vibrations of elastically embedded membranes made from DWCNTs according to the NRBM are derived:

$$\begin{aligned}
&\overline{\Lambda}\left\{\begin{array}{c}
(\varrho_1^2\delta_{j2} + \delta_{j1})\frac{\partial^2 \overline{v}_j^R}{\partial \tau^2} - \frac{(\varrho_2^2\delta_{j2} + \delta_{j1})}{\lambda_1^2}\frac{\partial^4 \overline{v}_j^R}{\partial \tau^2 \partial \xi^2} + \overline{S}_{vy_{(j+2,5-j)}}^R(\overline{v}_j^R - \overline{v}_{3-j}^R) \\
+\overline{S}_{vy_{(j+2,2)}}^R\left(2(\overline{v}_j^R - \overline{v}_{3-j}^R) - \overline{d}^2\frac{\partial^2 \overline{v}_{3-j}^R}{\partial \gamma^2} - \frac{\overline{d}^4}{12}\frac{\partial^4 \overline{v}_{3-j}^R}{\partial \gamma^4} - \frac{\overline{d}^6}{360}\frac{\partial^6 \overline{v}_{3-j}^R}{\partial \gamma^6}\right) \\
-\overline{S}_{vy_{(j+2,1)}}^R\left(\overline{d}^2\frac{\partial^2 \overline{v}_j^R}{\partial \gamma^2} + \frac{\overline{d}^4}{12}\frac{\partial^4 \overline{v}_j^R}{\partial \gamma^4} + \frac{\overline{d}^6}{360}\frac{\partial^6 \overline{v}_j^R}{\partial \gamma^6}\right) + \left(\overline{K}_t^R \overline{v}_j^R - \overline{K}_r^R \frac{\partial^2 \overline{v}_j^R}{\partial \xi^2}\right)(1 - \delta_{j1})
\end{array}\right\} \\
&+ (\varrho_3^2\delta_{j2} + \delta_{j1})\frac{\partial^4 \overline{v}_j^R}{\partial \xi^4} = 0,
\end{aligned} \tag{30a}$$

$$\overline{\Lambda}\left\{\begin{array}{c}(\varrho_1^2\delta_{j2}+\delta_{j1})\dfrac{\partial^2\overline{w}_j^R}{\partial\tau^2}-\dfrac{(\varrho_2^2\delta_{j2}+\delta_{j1})}{\lambda_1^2}\dfrac{\partial^4\overline{w}_j^R}{\partial\tau^2\partial\xi^2}+\overline{S}^R_{vz_{(j+2,5-j)}}(\overline{w}_j^R-\overline{w}^R_{3-j})\\ +\overline{S}^R_{vz_{(j+2,2)}}\left(2(\overline{w}_j^R-\overline{w}^R_{3-j})-\overline{d}^2\dfrac{\partial^2\overline{w}^R_{3-j}}{\partial\gamma^2}-\dfrac{\overline{d}^4}{12}\dfrac{\partial^4\overline{w}^R_{3-j}}{\partial\gamma^4}-\dfrac{\overline{d}^6}{360}\dfrac{\partial^6\overline{w}^R_{3-j}}{\partial\gamma^6}\right)\\ -\overline{S}^R_{vz_{(j+2,1)}}\left(\overline{d}^2\dfrac{\partial^2\overline{w}_j^R}{\partial\gamma^2}+\dfrac{\overline{d}^4}{12}\dfrac{\partial^4\overline{w}_j^R}{\partial\gamma^4}+\dfrac{\overline{d}^6}{360}\dfrac{\partial^6\overline{w}_j^R}{\partial\gamma^6}\right)+\left(\overline{K}_t^R\overline{w}_j^R-\overline{K}_r^R\dfrac{\partial^2\overline{w}_j^R}{\partial\xi^2}\right)(1-\delta_{j1})\end{array}\right\}$$
$$+(\varrho_3^2\delta_{j2}+\delta_{j1})\frac{\partial^4\overline{w}_j^R}{\partial\xi^4}=0. \tag{30b}$$

In extracting equations (30*a*) and (30*b*), it is noticed that the coefficients of the vdW forces between the innermost tubes of each pair of adjacent DWCNTs are the same. The same story holds true for coefficients of vdW forces between outermost tubes and innermost–outermost tubes of doubly neighboring DWCNTs. In other words,

$$S_{[\circ]_{(2n-2+j,2n-2)}}=S_{[\circ]_{(2n-2+j,2n+2)}}=S_{[\circ]_{(j+2,2)}},\ \ S_{[\circ]_{(2n-2+j,2n-3)}}=S_{[\circ]_{(2n-2+j,2n+1)}}=S_{[\circ]_{(j+2,1)}}, \tag{31}$$

where $[\circ]=vy$ or vz.

Equations (30*a*) and (30*b*) display dimensionless-continuous equations of motion of elastically confined membranes of DWCNTs on the basis of the NRBM.

3.1.2. Determination of natural frequencies. For a membrane with simply supported nanotubes whose exterior nanotubes are fixed transversely, the deflections of the continuous model are expressed in terms of the admissible mode shapes as follows:

$$\langle\overline{v}_j^R(\xi,\gamma,\tau),\overline{w}_j^R(\xi,\gamma,\tau)\rangle=\sum_{m=1}^{\infty}\sum_{n=1}^{\infty}\langle\overline{v}^R_{(mn0)_j}\,\mathrm{e}^{\mathrm{i}\bar{\omega}_y^R\tau},\overline{w}^R_{(mn0)_j}\,\mathrm{e}^{\mathrm{i}\bar{\omega}_z^R\tau}\rangle\sin(m\pi\xi)\sin(n\pi\gamma), \tag{32}$$

where $\overline{v}^R_{(mn0)_j}$ and $\overline{w}^R_{(mn0)_j}$ denote the dimensionless amplitudes, $\bar{\omega}_y^R$ and $\bar{\omega}_z^R$ represent the dimensionless flexural frequencies of the y- and z-directional vibrations of vertically aligned membranes of DWCNTs, respectively. By substituting equation (32) into equations (30*a*) and (30*b*), the natural frequencies of the nanosystem could be readily computed. The procedure of assessing the dimensionless flexural frequencies for the suggested model have been explicitly explained in the supplementary material, part C.

3.2. Application of the NTBM for continuous modeling of membranes of DWCNTs

3.2.1. Nonlocal-continuous equations of motion. By substituting equation (29) into equations (21)–(23) in view of equations (24), (28*a*)–(28*e*), the dimensionless governing equations of the elastically embedded nanosystem that display its transverse vibrations based on the continuous version of the NTBM take the following form:

$$\bar{\Lambda}\left\{\frac{(\varrho_2^2\delta_{j2}+\delta_{j1})}{\lambda_1^2}\frac{\partial^2\overline{\theta}_{z_j}^T}{\partial\tau^2}+\overline{K}_r^T\overline{\theta}_{z_j}^T(1-\delta_{j1})\right\}-(\varrho_4^2\delta_{j2}+\delta_{j1})\left(\frac{\partial\overline{v}_j^T}{\partial\xi}-\overline{\theta}_{z_j}^T\right)-(\varrho_3^2\delta_{j2}+\delta_{j1})\eta\frac{\partial^2\overline{\theta}_{z_j}^T}{\partial\xi^2}=0, \tag{33a}$$

$$\bar{\Lambda}\left\{\begin{array}{c}(\varrho_1^2\delta_{j2}+\delta_{j1})\dfrac{\partial^2\overline{v}_j^T}{\partial\tau^2}+\overline{S}^T_{vy_{(j+2,5-j)}}(\overline{v}_j^T-\overline{v}^T_{3-j})+\\ \overline{S}^T_{vy_{(j+2,2)}}\left(2(\overline{v}_j^T-\overline{v}^T_{3-j})-\overline{d}^2\dfrac{\partial^2\overline{v}^T_{3-j}}{\partial\gamma^2}-\dfrac{\overline{d}^4}{12}\dfrac{\partial^4\overline{v}^T_{3-j}}{\partial\gamma^4}-\dfrac{\overline{d}^6}{360}\dfrac{\partial^6\overline{v}^T_{3-j}}{\partial\gamma^6}\right)\\ -\overline{S}^T_{vy_{(j+2,1)}}\left(\overline{d}^2\dfrac{\partial^2\overline{v}_j^T}{\partial\gamma^2}+\dfrac{\overline{d}^4}{12}\dfrac{\partial^4\overline{v}_j^T}{\partial\gamma^4}+\dfrac{\overline{d}^6}{360}\dfrac{\partial^6\overline{v}_j^T}{\partial\gamma^6}\right)+\overline{K}_t^T\overline{v}_j^T(1-\delta_{j1})\end{array}\right\}-(\varrho_4^2\delta_{j2}+\delta_{j1})\left(\frac{\partial^2\overline{v}_j^T}{\partial\xi^2}-\frac{\partial\overline{\theta}_{z_j}^T}{\partial\xi}\right)=0, \tag{33b}$$

$$\bar{\Lambda}\left\{\frac{(\varrho_2^2\delta_{j2}+\delta_{j1})}{\lambda_1^2}\frac{\partial^2\overline{\theta}_{y_j}^T}{\partial\tau^2}+\overline{K}_r^T\overline{\theta}_{y_j}^T(1-\delta_{j1})\right\}-(\varrho_4^2\delta_{j2}+\delta_{j1})\left(\frac{\partial\overline{w}_j^T}{\partial\xi}-\overline{\theta}_{y_j}^T\right)-(\varrho_3^2\delta_{j2}+\delta_{j1})\eta\frac{\partial^2\overline{\theta}_{y_j}^T}{\partial\xi^2}=0, \tag{33c}$$

$$\bar{\Lambda}\left\{\begin{array}{c}(\varrho_1^2\delta_{j2}+\delta_{j1})\dfrac{\partial^2\overline{w}_j^T}{\partial\tau^2}+\overline{S}^T_{vz_{(j+2,5-j)}}(\overline{w}_j^T-\overline{w}_{3-j}^T)+\\ \overline{S}^T_{vz_{(j+2,2)}}\left(2(\overline{w}_j^T-\overline{w}_{3-j}^T)-\overline{d}^2\dfrac{\partial^2\overline{w}_{3-j}^T}{\partial\gamma^2}-\dfrac{\overline{d}^4}{12}\dfrac{\partial^4\overline{w}_{3-j}^T}{\partial\gamma^4}-\dfrac{\overline{d}^6}{360}\dfrac{\partial^6\overline{w}_{3-j}^T}{\partial\gamma^6}\right)\\ -\overline{S}^T_{vz_{(j+2,1)}}\left(\overline{d}^2\dfrac{\partial^2\overline{w}_j^T}{\partial\gamma^2}+\dfrac{\overline{d}^4}{12}\dfrac{\partial^4\overline{w}_j^T}{\partial\gamma^4}+\dfrac{\overline{d}^6}{360}\dfrac{\partial^6\overline{w}_j^T}{\partial\gamma^6}\right)+\overline{K}_t^T\overline{w}_j^T(1-\delta_{j1})\end{array}\right\}-(\varrho_4^2\delta_{j2}+\delta_{j1})\left(\frac{\partial^2\overline{w}_j^T}{\partial\xi^2}-\frac{\partial\overline{\theta}_{y_j}^T}{\partial\xi}\right)=0. \quad (33d)$$

3.2.2. Determination of natural frequencies. By taking into account the given boundary conditions in section 3.1.2, the deflections and their angles for the proposed continuous-based model using NTBM could be written in terms of admissible modes as follows:

$$\langle\overline{v}_j^T(\xi,\gamma,\tau),\overline{w}_j^T(\xi,\gamma,\tau)\rangle=\sum_{m=1}^{\infty}\sum_{n=1}^{\infty}\langle\overline{v}^T_{(mn0)_j}\,e^{i\bar{\omega}_y^T\tau},\overline{w}^T_{(mn0)_j}\,e^{i\bar{\omega}_z^T\tau}\rangle\sin(m\pi\xi)\sin(n\pi\gamma), \quad (34a)$$

$$\langle\overline{\theta}_{z_j}^T(\xi,\gamma,\tau),\overline{\theta}_{y_j}^T(\xi,\gamma,\tau)\rangle=\sum_{m=1}^{\infty}\sum_{n=1}^{\infty}\langle\overline{\theta}^T_{z(mn0)_j}\,e^{i\bar{\omega}_y^T\tau},\overline{\theta}^T_{y(mn0)_j}\,e^{i\bar{\omega}_z^T\tau}\rangle\cos(m\pi\xi)\sin(n\pi\gamma), \quad (34b)$$

in which $\overline{v}^T_{(mn0)_j}$, $\overline{w}^T_{(mn0)_j}$, $\overline{\theta}^T_{z(mn0)_j}$, and $\overline{\theta}^T_{y(mn0)_j}$ represent the unknown coefficients of vibrational modes, $\bar{\omega}_y^T$ and $\bar{\omega}_z^T$ are the dimensionless natural frequencies of the vertically aligned membrane, respectively. Finally, by substituting equations (34*a*)–(34*b*) into equations (33*a*)–(33*d*), the fundamental frequencies for each direction are calculated. The details of the carried out calculations are provided in the supplementary material, part D.

4. Results and discussion

In this section, the results of parametric studies of free vibration of elastically embedded membranes made of DWCNTs are presented according to the proposed NRBM and NTBM. The influences of important factors including the small-scale parameter, the number of constitutive double-walled nanotubes, the radius, the intertube distance, the slenderness ratio of the nanotubes, and their elastodynamic interactions with the surrounding matrix on the natural frequencies are going to be studied. For this purpose, the geometrical and mechanical properties of the nanosystem are considered as in the following form: $r_{m_1}=1$ nm, $l_s=2$ nm, $\nu_b=0.2$, $r_{m_2}=r_{m_1}+th$, $d=2r_{m_2}+th$, $E_b=1$ TPa, $th=0.34$ nm, and $\rho_b=2300\ \mathrm{kg\ m^{-3}}$. In the provided numerical examinations, the interactions of the nanosystem with the elastic bed have been ignored (i.e. $K_t=K_r=0$), except the cases that the values of such factors have been explicitly stated.

In tables 1 and 2, the results of the nonlocal continuous and discrete models (NCMs and NDMs) according to the NRBM and NTBM are presented. The results of these models are compared with each other for membranes with various populations and three values of the nonlocal parameter. The obtained results show that the NCMs can predict those of the NDMs with a small relative error. In the continuous modeling of the problem, increasing the number of nanotubes does not influence on the computational costs seriously. This implies that the NCMs can be efficiently employed for estimating the overall vibration behavior of the nanoscaled systems with high populations. Further examination of the results also reveals that by increasing the nonlocal factor or by growing the number of tubes, the fundamental frequencies reduce. The results of the Timoshenko's theory for both NCMs and NDMs are less than those of the Rayleigh beam theory. The main reason for such a behavior is related to the consideration of the shear strain energy by the Timoshenko beam theory.

In table 3, the effect of transverse and rotational stiffness of the surrounding environment on the fundamental frequencies of the nanosystem is presented for different lengths. To this end, the parameters $K_t^{*R}=\left(\frac{l_b^*}{l_b}\right)^4\bar{K}_t^R$, $K_r^{*R}=\left(\frac{l_b^*}{l_b}\right)^2\bar{K}_r^R$, and $l_b^*=12$ nm are used. These factors are defined such that the length dependency of the transverse and rotational stiffness is removed. The results of the NCMs represent a very good approximation of the NDMs' results for different lengths and stiffness. Through growing of the elastic stiffness of the surrounding environment, the fundamental frequency of the nanoscaled system increases. Such a fact is more obvious in nanosystems with higher lengths. Also, the presented results indicate that increasing the length of DWCNTs yields reducing fundamental frequencies. Given the relatively good results of the NCMs in compare to the results of the NDMs, we use continuous models for conducting parametric studies in the remainder of this work.

Given the crucial role of the nonlocal factor in the nanosystem vibrations, the plots of the fundamental frequencies of lateral vibrations as a function of the nonlocal parameter are provided in figure 4. The results are plotted for a membrane consists of 200 DWCNTs and three slenderness ratios. It is observed that the frequencies of the vibrations in lateral directions would reduce by increasing the nonlocal parameter. The reason for such behavior can be related to the reduction of the ratio of lateral stiffness to the mass due to an

Table 1. The estimated fundamental frequencies of the nanoscaled system vibrating in the y direction by employing the NDMs and NCMs ($\lambda_1 = 16$).

	l_s (nm)	$N = 5$	$N = 8$	$N = 10$	$N = 15$	$N = 20$	$N = 30$
DMs[a]							
NRBM	0	1.583 724	1.408 726	1.370 890	1.335 468	1.323 758	1.315 730
	1	1.545 686	1.365 720	1.326 636	1.289 981	1.277 847	1.269 525
	2	1.454 075	1.260 844	1.218 347	1.178 278	1.164 965	1.155 818
NTBM	0	1.478 201	1.284 440	1.241 877	1.201 766	1.188 445	1.179 293
	1	1.445 540	1.246 642	1.202 726	1.161 249	1.147 452	1.137 968
	2	1.367 168	1.154 671	1.107 075	1.061 831	1.046 712	1.036 298
CMs[a]							
NRBM	0	1.583 751	1.408 732	1.370 892	1.335 469	1.323 759	1.315 730
	1	1.545 714	1.365 726	1.326 639	1.289 982	1.277 848	1.269 525
	2	1.454 105	1.260 851	1.218 351	1.178 279	1.164 965	1.155 818
NTBM	0	1.478 230	1.284 447	1.241 881	1.201 767	1.188 445	1.179 294
	1	1.445 570	1.246 648	1.202 730	1.161 250	1.147 453	1.137 968
	2	1.367 199	1.154 678	1.107 078	1.061 832	1.046 713	1.036 298

[a] DMs and CMs stand for discrete models and continuous models, respectively.

Table 2. The estimated fundamental frequencies of the nanoscaled system vibrating in the z direction by employing the NDMs and NCMs ($\lambda_1 = 16$).

	l_s (nm)	$N = 5$	$N = 8$	$N = 10$	$N = 15$	$N = 20$	$N = 30$
DMs							
NRBM	0	1.316 675	1.312 028	1.311 097	1.310 250	1.309 975	1.309 788
	1	1.270 503	1.265 684	1.264 719	1.263 841	1.263 555	1.263 361
	2	1.156 890	1.151 591	1.150 530	1.149 563	1.149 250	1.149 036
NTBM	0	1.180 363	1.175 064	1.174 002	1.173 036	1.172 722	1.172 508
	1	1.139 075	1.133 582	1.132 481	1.131 479	1.131 153	1.130 932
	2	1.037 512	1.031 474	1.030 264	1.029 161	1.028 803	1.028 563
CMs							
NRBM	0	1.316 675	1.312 028	1.311 097	1.310 250	1.309 975	1.309 788
	1	1.270 503	1.265 684	1.264 719	1.263 841	1.263 555	1.263 361
	2	1.156 890	1.151 591	1.150 530	1.149 563	1.149 250	1.149 036
NTBM	0	1.180 363	1.175 064	1.174 002	1.173 036	1.172 722	1.172 508
	1	1.139 076	1.133 582	1.132 481	1.131 479	1.131 153	1.130 932
	2	1.037 512	1.031 474	1.030 264	1.029 161	1.028 80	1.028 560

increase of the nonlocal parameter. As it can be seen, the effect of this parameter on nanosystems with higher slenderness ratio is more apparent. In other words, by growing of the slenderness ratio, variation of the nonlocal factor would have less influence on the variation of the fundamental frequencies. As shown in figure 4, the estimated results by the NRBM are higher than those estimated by the NTBM. For $\lambda_1 = 8$ and 18, the relative error between the results of the NRBM and those of the NTBM are about 34% and 10%, respectively. Actually, the NRBM-based plotted results approach to those obtained on the basis of the NTBM as the slenderness ratio magnifies.

In figure 5, the fundamental frequencies of the vertically aligned DWCNTs for both lateral vibrations are depicted in terms of the number of nanotubes. The results of the continuous models based on the NRBM and NTBM for isolated nanosystems from the surrounding elastic medium are given for the three values of the slenderness ratio (i.e. $\lambda = 8$, 16 and 24). The demonstrated results show that the z-directional fundamental frequency, especially for a nanosystem with a lower number of nanotubes, is greater than the y-directional frequency. The reason for this is the stronger vdW force is in the z direction with respect to that in the y direction, which results in more in-plane stiffness. Additionally, by an increase

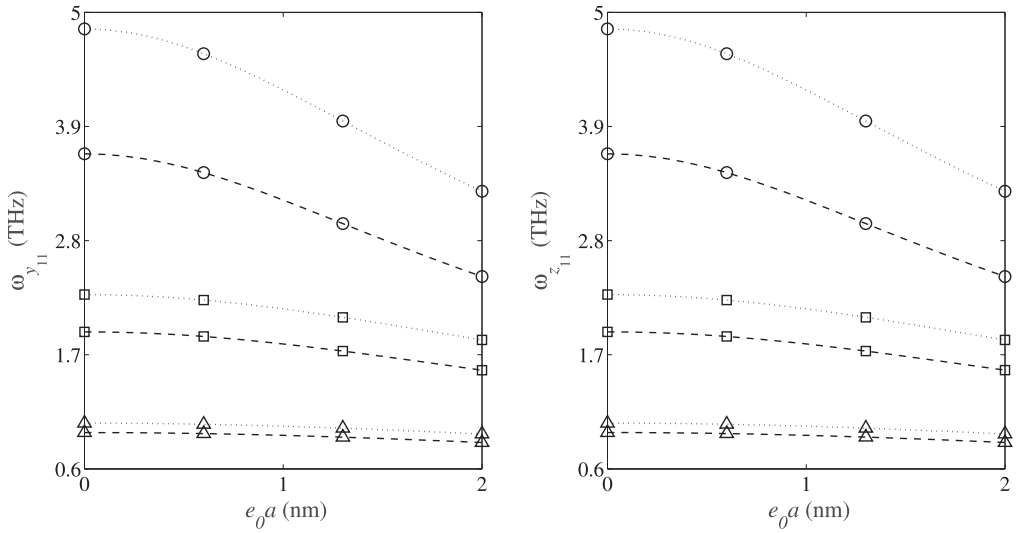

Figure 4. Effect of the nonlocal parameter on the bilateral fundamental frequencies for different values of the slenderness ratio: (…) NRBM, (—) NTBM; (∘) $\lambda_1 = 8$, (□) $\lambda_1 = 12$, (Δ) $\lambda_1 = 18$; $N = 200$.

Table 3. The estimated fundamental frequencies of the elastically confined nanoscaled system vibrating in the z direction using NDMs and NCMs for different levels of the nanotube's length and various values of the transverse and rotational stiffness of the nearby medium ($N = 30$, $K_t^{*R} = \left(\frac{l_b^*}{l_b}\right)^4 \overline{K}_t^R$, $K_r^{*R} = \left(\frac{l_b^*}{l_b}\right)^2 \overline{K}_r^R$, $l_b^* = 12$ nm).

	l_b	$K_r^* = 0$			$K_t^* = 0$		
	(nm)	$K_t^* = 0$	$K_t^* = 50$	$K_t^* = 100$	$K_r^* = 0$	$K_r^* = 50$	$K_r^* = 100$
	l_b		$K_r^{*R} = 0$			$K_t^{*R} = 0$	
	(nm)	$K_t^{*R} = 0$	$K_t^{*R} = 50$	$K_t^{*R} = 100$	$K_r^{*R} = 0$	$K_r^{*R} = 50$	$K_r^{*R} = 100$
DMs							
NRBM	8	2.064 9440	2.113 5242	2.160 8745	2.064 9440	2.937 6515	3.562 8723
	10	1.453 6491	1.525 0220	1.593 0030	1.453 6491	2.252 7953	2.812 0608
	12	1.071 2313	1.168 5448	1.258 0970	1.071 2313	1.808 3677	2.308 4278
NTBM	8	1.708 3565	1.770 8211	1.830 9642	1.708 3565	2.018 6769	2.142 7654
	10	1.268 4307	1.352 3444	1.431 1027	1.268 4307	1.613 6828	1.746 3209
	12	0.968 0621	1.076 6377	1.174 9278	0.968 0621	1.330 0893	1.463 5568
CMs							
NRBM	8	2.064 9440	2.113 5243	2.160 8745	2.064 9440	2.937 6515	3.562 8723
	10	1.453 6492	1.525 0221	1.593 0031	1.453 6492	2.252 7953	2.812 0609
	12	1.071 2315	1.168 5449	1.258 0971	1.071 2315	1.808 3678	2.308 4279
NTBM	8	1.708 3565	1.770 8212	1.830 9643	1.708 3565	2.018 6770	2.142 7655
	10	1.268 4308	1.352 3445	1.431 1028	1.268 4308	1.613 6829	1.746 3210
	12	0.968 0622	1.076 6378	1.174 9280	0.968 0622	1.330 0894	1.463 5569

of the number of nanotubes, the difference between the fundamental frequencies decreases. As it is observed in the plotted graphs, the in-plane frequency reduces by magnifying the number of nanotubes, which is more visible for membranes with a higher slenderness ratio. For out-of-plate vibrations, the fundamental frequency is less affected by the number of nanotubes. Further, the relative difference between two proposed models varies slightly with increasing of the number of nanotubes. Considering the effect of shear deformation in the NTBM, as the graphs show, NTBM's plots are lower than those of the NRBM. According to the plotted results, the NRBM can generate the NTBM's results for the slenderness ratios of 8 and 24 with relative errors of less than 34% and 6%, respectively.

In this part, the role of the slenderness ratio in the nanosystem's free dynamic response are systematically examined. In figure 6, the frequencies associated with the lateral directions are plotted for membranes with 7, 10, and 30 DWCNTs using proposed nonlocal continuous models. It is revealed from the demonstrated graphs that growing of the

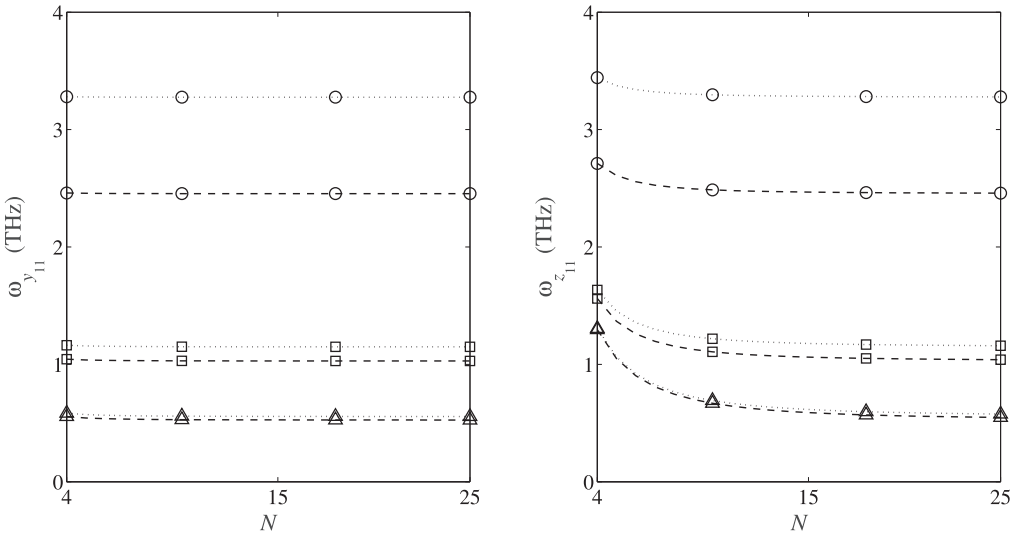

Figure 5. Effect of the number of nanotubes on the bilateral fundamental frequencies for different levels of the slenderness ratio: (…) NRBM, (—) NTBM; (∘) $\lambda_1 = 8$, (□) $\lambda_1 = 16$, (Δ)$\lambda_1 = 24$.

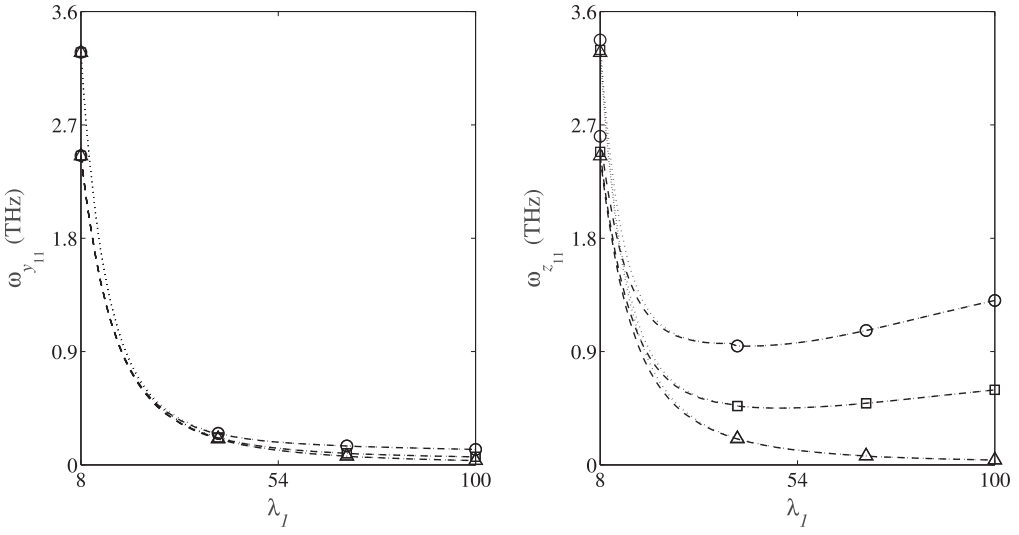

Figure 6. Effect of the slenderness ratio on the bilateral fundamental frequencies for different numbers of nanotubes: (…) NRBM, (—) NTBM; (∘) $N = 5$, (□) $N = 10$, (Δ) $N = 30$; $l_s = 2$ nm.

slenderness ratio leads to the decreasing of the fundamental frequencies. In contrast to the results of the out-of-plane vibrations, the in-plane fundamental frequency of nanosystems follows a decreasing trend for $\lambda < 45$. By magnifying the slenderness ratio in the range of $\lambda > 45$, the estimated frequencies by both NRBM and NTBM grow with a moderate slope. This issue becomes more pronounced for vertically aligned membranes of DWCNTs with lower numbers of nanotubes. Such a vibrational behavior is related to the strengthening of the in-plane vdW forces by increasing of the slenderness ratio. Actually for the increasing branches of the plots, the reduction effect of frequencies by a growth of the slenderness ratio is lesser than the increasing effect of the natural frequencies due to the growth of the vdW forces. According to the presented results, for low slenderness ratios, the NRBM's frequencies are higher than those of the NTBM. As this ratio increases, the differences between the results of the NRBM and those of the NTBM would reduce. Such a trend action is mainly related to the greater impact of the shear deformation on the fundamental frequencies in the lower slenderness ratios. On the other hand, in vertically aligned membranes of DWCNTs with low slenderness ratios, the effect of the number of nanotubes on their free vibration is fairly negligible.

One of the parameters affecting nanosystem vibrations is the distance between nanotubes. In figures 7(a)–(c), the influence of the nanotubes spacing on the fundamental frequencies for three small-scale factors (i.e. $e_0a = 0$, 1 and 2 nm), and membranes consisting of 5, 10, and 20 DWCNTs have been investigated. The intertube distance varies from $2r_{m_1} + 3th$ to $2r_{m_1} + 5th$. By examining the results, it is found that the fundamental frequency pertinent to vibration in z direction decreases by increasing of the intertube distance up to $2r_{m_1} + 3.2th$. The reason for such a complex behavior can

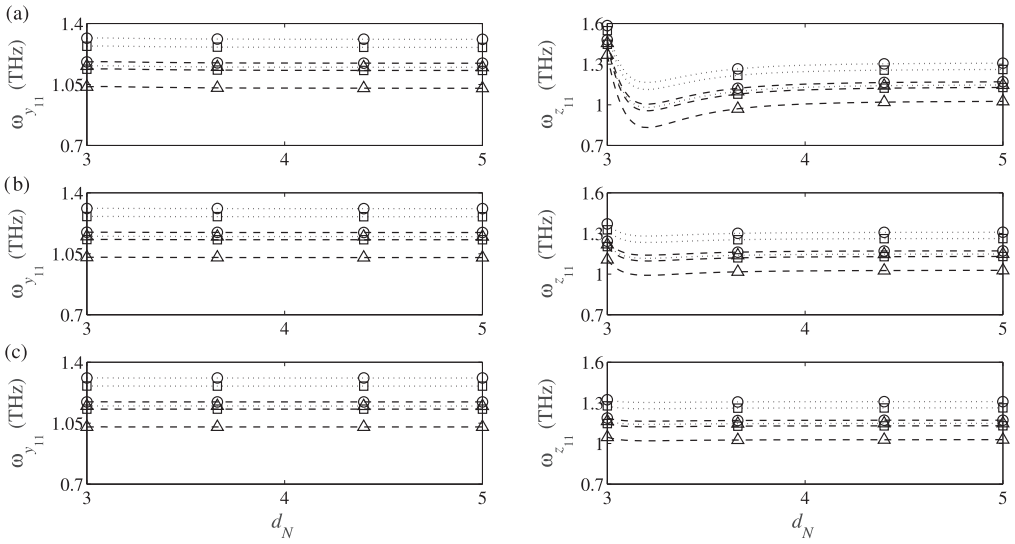

Figure 7. Effect of the intertube space on the bilateral fundamental frequencies for different nonlocal parameters: (…) NRBM, (—) NTBM; (*a*) $N = 5$, (*b*) $N = 10$, (*c*) $N = 20$; (∘) $l_s = 0$, (□) $l_s = 1$, (Δ) $l_s = 2$ nm; $\lambda_1 = 15$, $d_N = \frac{d - 2r_{m_1}}{th}$.

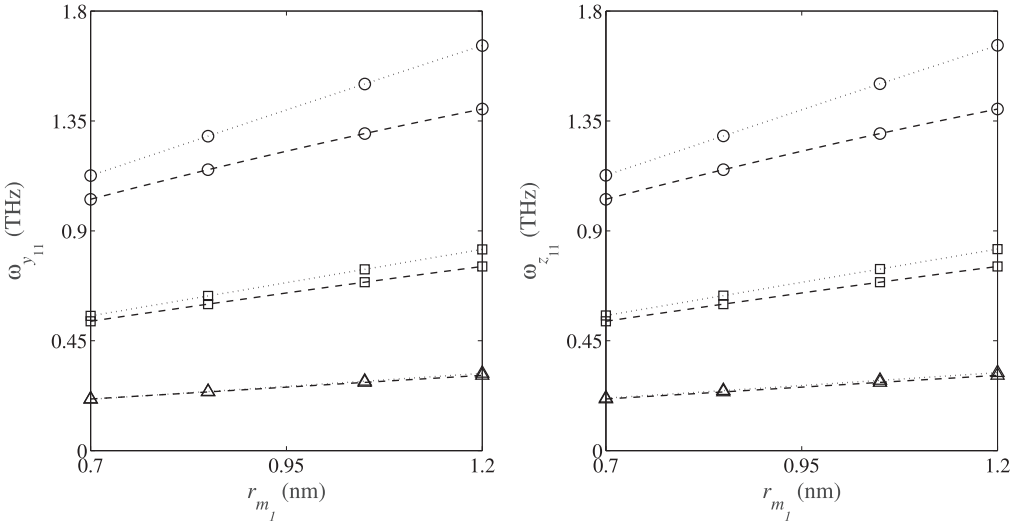

Figure 8. Effect of the radius of consisting nanotubes on the bilateral fundamental frequencies for different lengths: (…) NRBM, (—) NTBM; (∘) $l_b = 10$, (□) $l_b = 15$, (Δ)$l_b = 25$ nm; $N = 100$.

be attributed to the reduction of the coefficient of vdW forces by enlarging the intertube distance up to $2r_{m_1} + 3.2th$. Subsequently, as such a distance grows more, the vdW force would also develop gradually, resulting in an increase in the fundamental frequency. As the intertube distance becomes greater than $2r_{m_1} + 4th$, the vdW force and the frequency vary slightly due to the variation of the intertube distance. In fact, for relatively large intertube distances, the dynamic interactions of nanotubes would lessen, and each nanotube vibrates almost independently from its neighboring nanotubes. Unlike the *z*-directional results, the vdW force along the *y* direction would vary slightly by growing the intertube distance, so its corresponding fundamental frequency first increases slightly and then goes on steady. As the graphs in figures 7(b) and (c) display, with increasing the number of nanotubes, both laterally fundamental frequencies as well as their variations in terms of the intertube distance would reduce. This fact is so obvious in figure 7(c).

Another parameter whose influence on the free transverse dynamic response of the vertically aligned single-layered DWCNTs is going to be discussed is the mean radius of the consisting nanotubes. In figure 8, the graphs of such frequency are plotted for vibrations in two directions, *y* and *z*. The obtained results are for membranes consist of DWCNTs with three lengths of 10, 15 and 25 nm. According to the plotted results, the frequencies of both lateral directions rise by growing of the mean radius of the consisting nanotubes, which is clearly seen in short-length nanotubes. Due to the fact that the coefficient of the in-plane vdW forces and the flexural stiffness of the consisting nanostructures increase with the increase of the nanotube radius, the increase in the fundamental frequencies due to the increase in the nanotube's

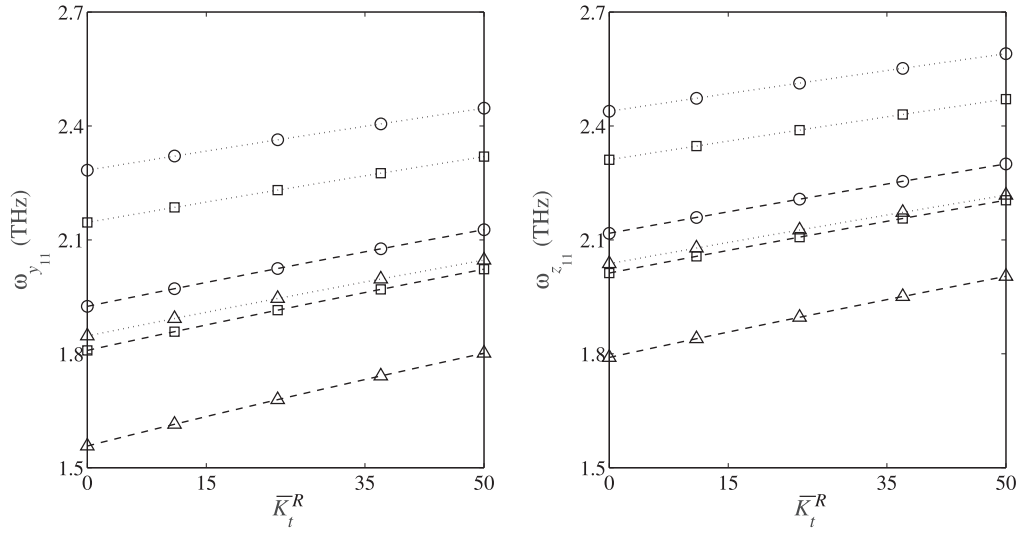

Figure 9. Effect of the matrix's transverse stiffness on the bilateral fundamental frequencies for different nonlocal parameters: (…) NRBM, (—) NTBM; (∘) $l_s = 0$, (□) $l_s = 1$, (Δ) $l_s = 2$ nm; $K_r = 0$, $N = 5$, $\lambda_1 = 12$.

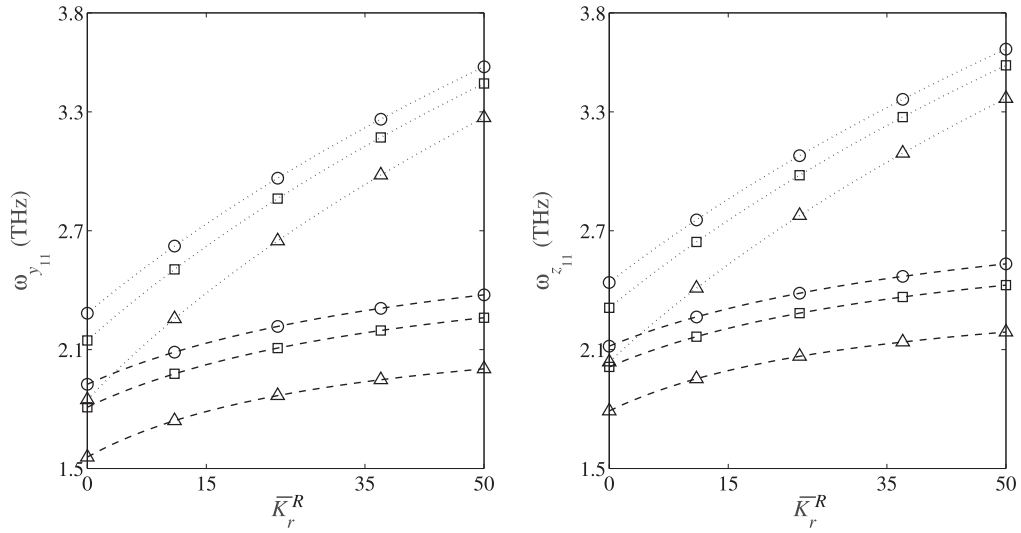

Figure 10. Effect of the matrix's rotational stiffness on the bilateral fundamental frequencies for different nonlocal parameters: (…) NRBM, (—) NTBM; (∘) $l_s = 0$, (□) $l_s = 1$, (Δ) $l_s = 2$ nm; $K_t = 0$, $N = 5$, $\lambda_1 = 12$.

radius is interpreted. On the other hand, by enlarging the length of the nanotubes, the growth rate of the fundamental frequencies decreases, and the relative difference between the results of the suggested models lessens (for example, in the case of $l_b = 25$ nm, these differences are lesser than 4%).

In this part, only the effect of the transverse stiffness of the matrix ($K_r = 0$) on the fundamental frequencies of the vertically aligned membranes of DWCNTs is of interest. As shown in figure 9, the increase in the lateral stiffness yields an increase of the total stiffness of the elastically embedded nanosystem, which increases the fundamental frequencies of the nanostructure. Further investigations reveal that due to the presence of stronger vdW force in the z direction, the in-plane frequencies are commonly greater than the out-of-plate frequencies. Increasing of the small-scale parameter also reduces the fundamental frequencies, irrespective of the transverse stiffness of the surrounding matrix. Generally, the NTBM's results are lower than the NRBM's results. The in-plane vibrational analyses of the nanosystem show that in the case of $K_t = 0$ and for three levels of the small-scale parameter ($e_0a = 0$, 1, and 2 nm), the NRBM can reproduce the results of the NTBM with relative error lower than 15.5%, 15% and 14% respectively. While in the case of $\bar{K}_t^R = 50$, such relative errors approach 19%, 18.5% and 16.5%, respectively.

Herein, the effect of rotational stiffness of the matrix on free vibration behavior of the nanosystem is examined. In figure 10, the fundamental frequencies as a function of rotational stiffness of the surrounding medium have been demonstrated when the transverse stiffness of the matrix is set equal to zero. As it can be seen, the fundamental frequencies of the nanostructure would grow as the rotational stiffness increases. It means that increasing of the rotational stiffness of the matrix leads to an increase of

the whole lateral stiffness of the elastically embedded nanosystem. The rate of variation of the predicted frequencies by the NRBM, in contrast to the other model, is more rapid. Further, the role of stiffness of the nanoscale system on the free vibration on the basis of the NRBM is more noticeable than that of the NTBM. In this section, as with previous results, the results of the NRBM model are higher than the NTBM model. In addition, the increase in the small-scale parameter leads to the reduction of the fundamental frequencies for all considered values of the rotational stiffness. The obtained results of the in-plane vibrational analysis indicate that for $K_r = 0$, and at each considered level of the small-scale parameter (i.e. $e_0a = 0$, 1 and 2), the NRBM model could generate the results of the NTBM with relative errors lower than 16%, 15% and 14%, respectively, while in the case of $\bar{K}_r = 50$, these relative errors in order are about 43%, 46% and 58% for the above-mentioned small-scale parameters.

The major advantages of the proposed models are as: (i) the high computational efforts of the atomistic-based approaches for mechanical analysis of the understudy nanosystem are extremely reduced by using nonlocal continuum-based models; (ii) the influences of both nonlocality and shear effects on the free vibration of the nanosystem are revealed and explained; (iii) the proposed nonlocal continuous models would be very useful for highly populated nanosystems in which the nonlocal discrete models suffer from high computational costs; (iv) the suggested models would be beneficial for optimal design of vertically membranes of DWCNTs since the presented graphs for the influences of various factors on its vibrational behavior are now clearly available. The main limitations of the presented models are as: (i) only linear and transverse vibrations of the nanosystem are addressed by the suggested models; (ii) the nonlinear terms of the dynamical part of the resultant van der Waals forces have been excluded; (iii) the inter-tube friction has not been taken into account in the lateral vibrations of the nanosystem. To fill these gaps, more sophisticated models should be developed by researchers in the field of applied physical/mechanical sciences.

5. Concluding remarks

The transverse free dynamic response of vertically aligned single-layered DWCNTs embedded in an elastic matrix were investigated in some detail. In the context of the nonlocal elasticity theory of Eringen, the vibrational behavior of the nanosystem was modeled using both discrete and continuous models. The results show that the continuous models can appropriately reproduce the natural frequencies of the discrete models. The efficiency of the suggested continuous models in estimating fundamental frequencies of nanosystems with a high number of DWCNTs is proved numerically and explained. The influences of crucial geometry parameters, nonlocality, and matrix's stiffness on the natural frequencies were displayed in some detail. The importance of the shear deformation effect on the free dynamic response was also highlighted and explained.

The suggested models can be also exploited for the nonlocal vibrational analysis of more complex configurations, including orthogonal membranes as well as three-dimensional jungles of vertically aligned DWCNTs. The work on these hot topics can be followed by interested scholars and investigators in the near future.

Acknowledgments

The financial supports of the Iran National Science Foundation (INSF) as well as K N Toosi University of Technology from the undertaken work are highly appreciated.

ORCID iDs

Keivan Kiani https://orcid.org/0000-0003-0962-009X

References

[1] Zhou C, Kumar S, Doyle C D and Tour J M 2005 Functionalized single wall carbon nanotubes treated with pyrrole for electrochemical supercapacitor membranes *Chem. Mater.* **17** 1997–2002
[2] Fang Y, Liu J, Yu D J, Wicksted J P, Kalkan K, Topal C O, Flanders B N, Wu J and Li J 2010 Self-supported supercapacitor membranes: polypyrrole-coated carbon nanotube networks enabled by pulsed electrodeposition *J. Power Sources* **195** 674–9
[3] Kaempgen M, Chan C K, Ma J, Cui Y and Gruner G 2009 Printable thin film supercapacitors using single-walled carbon nanotubes *Nano Lett.* **9** 1872–6
[4] Che G, Lakshmi B B, Fisher E R and Martin C R 1998 Carbon nanotubule membranes for electrochemical energy storage and production *Nature* **393** 346–9
[5] Wang C, Waje M, Wang X, Tang J M, Haddon R C and Yan Y 2004 Proton exchange membrane fuel cells with carbon nanotube based electrodes *Nano Lett.* **4** 345–8
[6] Rajalakshmi N, Ryu H, Shaijumon M M and Ramaprabhu S 2005 Performance of polymer electrolyte membrane fuel cells with carbon nanotubes as oxygen reduction catalyst support material *J. Power Sources* **140** 250–7
[7] Wu Z *et al* 2004 Transparent, conductive carbon nanotube films *Science* **305** 1273–6
[8] Murakami Y and Maruyama S 2006 Detachment of vertically aligned single-walled carbon nanotube films from substrates and their re-attachment to arbitrary surfaces *Chem. Phys. Lett.* **422** 575–80
[9] Liu P, Zhang Y W, Lu C and Lam K Y 2004 Tensile and bending properties of double-walled carbon nanotubes *J. Phys. D: Appl. Phys.* **37** 2358
[10] Damnjanovic M, Miloševic I, Dobardžic E, Vukovic T and Nikolic B 2004 Commensurate double-walled carbon nanotubes: symmetry and phonons *Phys. Rev.* B **69** 153401
[11] Colomer J F, Henrard L, Launois P, Tendeloo G V, Lucas A A and Lambin P H 2004 Bundles of identical double-walled carbon nanotubes *Chem. Commun.* **22** 2592–3
[12] Kajiura H, Huang H and Bezryadin A 2004 Quasi-ballistic electron transport in double-wall carbon nanotubes *Chem. Phys. Lett.* **398** 476–9
[13] Li Y, Wang K, Wei J, Gu Z, Wang Z, Luo J and Wu D 2005 Tensile properties of long aligned double-walled carbon nanotube strands *Carbon* **43** 31–5

[14] Cao A, Dickrell P L, Sawyer W G, Ghasemi-Nejhad M N and Ajayan P M 2005 Super-compressible foamlike carbon nanotube films *Science* **310** 1307–10

[15] Wang D, Song P, Liu C, Wu W and Fan S 2008 Highly oriented carbon nanotube papers made of aligned carbon nanotubes *Nanotechnology* **19** 075609

[16] Eringen A C and Edelen D G B 1972 On nonlocal elasticity *Int. J. Eng. Sci.* **10** 233–48

[17] Eringen A C 1972 Linear theory of nonlocal elasticity and dispersion of plane waves *Int. J. Eng. Sci.* **10** 425–35

[18] Eringen A C 1972 Nonlocal polar elastic continua *Int. J. Eng. Sci.* **10** 1–16

[19] Eringen A C 2002 *Nonlocal Continuum Field Theories* (New York: Springer)

[20] Duan W H, Wang C M and Zhang Y Y 2007 Calibration of nonlocal scaling effect parameter for free vibration of carbon nanotubes by molecular dynamics *J. Appl. Phys.* **101** 024305

[21] Zhang Y Y, Wang C M and Tan V B C 2009 Assessment of Timoshenko beam models for vibrational behavior of single-walled carbon nanotubes using molecular dynamics *Adv. Appl. Math. Mech.* **1** 89–106

[22] Ansari R, Rouhi H and Sahmani S 2011 Calibration of the analytical nonlocal shell model for vibrations of double-walled carbon nanotubes with arbitrary boundary conditions using molecular dynamics *Int. J. Mech. Sci.* **53** 786–92

[23] Kiani K 2016 Free dynamic analysis of functionally graded tapered nanorods via a newly developed nonlocal surface energy-based integro-differential model *Compos. Struct.* **139** 151–66

[24] Barretta R, Canadija M, Luciano R and de Sciarra F M 2018 Stress-driven modeling of nonlocal thermoelastic behavior of nanobeams *Int. J. Eng. Sci.* **126** 53–67

[25] Numanoglu H M, Akgoz B and Civalek O 2018 On dynamic analysis of nanorods *Int. J. Eng. Sci.* **130** 33–50

[26] Kiani K 2016 Nonlocal-integro-differential modeling of vibration of elastically supported nanorods *Physica* E **83** 151–63

[27] Hamza-Cherif R, Meradjah M, Zidour M, Tounsi A, Belmahi S and Bensattalah T 2018 Vibration analysis of nano beam using differential transform method including thermal effect *J. Nano Res.* **54** 1–14

[28] Youcef D O, Kaci A, Benzair A, Bousahla A A and Tounsi A 2018 Dynamic analysis of nanoscale beams including surface stress effects *Smart Struct. Sys.* **21** 65–74

[29] Bouadi A, Bousahla A A, Houari M S A, Heireche H and Tounsi A 2018 A new nonlocal HSDT for analysis of stability of single layer graphene sheet *Adv. Nano Res.* **6** 147–62

[30] Kadari B, Bessaim A, Tounsi A, Heireche H, Bousahla A A and Houari M S A 2018 Buckling analysis of orthotropic nanoscale plates resting on elastic foundations *J. Nano Res.* **55** 42–56

[31] Yazid M, Heireche H, Tounsi A, Bousahla A A and Houari M S A 2018 A novel nonlocal refined plate theory for stability response of orthotropic single-layer graphene sheet resting on elastic medium *Smart Struct. Sys.* **21** 15–25

[32] Artan R and Tepe A 2011 Nonlocal effects in curved single-walled carbon nanotubes *Mech. Adv. Mater. Struct.* **18** 347–51

[33] Fazelzadeh S A and Ghavanloo E 2012 Nonlocal anisotropic elastic shell model for vibrations of single-walled carbon nanotubes with arbitrary chirality *Compos. Struct.* **94** 1016–22

[34] Azrar A, Azrar L and Aljinaidi A A 2016 Analytical and numerical modeling of higher order free vibration characteristics of single-walled carbon nanotubes *Mech. Adv. Mater. Struct.* **23** 1245–62

[35] Karlicic D, Kozic P, Pavlovic R and Neic N 2017 Dynamic stability of single-walled carbon nanotube embedded in a viscoelastic medium under the influence of the axially harmonic load *Compos. Struct.* **162** 227–43

[36] Jiang J, Wang L and Zhang Y 2017 Vibration of single-walled carbon nanotubes with elastic boundary conditions *Int. J. Mech. Sci.* **122** 156–66

[37] Wang Q, Cui X, Qin B and Liang Q 2017 Vibration analysis of the functionally graded carbon nanotube reinforced composite shallow shells with arbitrary boundary conditions *Compos. Struct.* **182** 364–79

[38] Zghal S, Frikha A and Dammak F 2018 Free vibration analysis of carbon nanotube-reinforced functionally graded composite shell structures *Appl. Math. Model.* **53** 132–55

[39] Ebrahimi F and Dabbagh A 2018 NSGT-based acoustical wave dispersion characteristics of thermo-magnetically actuated double-nanobeam systems *Struct. Eng. Mech.* **68** 701–11

[40] Ebrahimi F, Dehghan M and Seyfi A 2019 Eringen's nonlocal elasticity theory for wave propagation analysis of magneto-electro-elastic nanotubes *Adv. Nano. Res.* **7** 1–11

[41] Wang Q and Varadan V K 2006 Vibration of carbon nanotubes studied using nonlocal continuum mechanics *Smart Mater. Struct.* **15** 659

[42] Zhang Y Q, Liu X and Liu G R 2007 Thermal effect on transverse vibrations of double-walled carbon nanotubes *Nanotechnology* **18** 445701

[43] Hu Y G, Liew K M, Wang Q, He X Q and Yakobson B I 2008 Nonlocal shell model for elastic wave propagation in single- and double-walled carbon nanotubes *J. Mech. Phys. Solids* **56** 3475–85

[44] Heireche H, Tounsi A and Benzair A 2008 Scale effect on wave propagation of double-walled carbon nanotubes with initial axial loading *Nanotechnology* **19** 185703

[45] Ansari R, Rouhi S and Shahnazari A 2018 Investigation of the vibrational characteristics of double-walled carbon nanotubes/double-layered graphene sheets using the finite element method *Mech. Adv. Mater. Struct.* **25** 253–65

[46] Murmu T, McCarthy M A and Adhikari S 2012 Vibration response of double-walled carbon nanotubes subjected to an externally applied longitudinal magnetic field: a nonlocal elasticity approach *J. Sound Vib.* **331** 5069–86

[47] Kiani K 2013 Characterization of free vibration of elastically supported double-walled carbon nanotubes subjected to a longitudinally varying magnetic field *Acta Mech.* **224** 3139–51

[48] Kiani K 2014 Longitudinally varying magnetic field influenced transverse vibration of embedded double-walled carbon nanotubes *Int. J. Mech. Sci.* **87** 179–99

[49] Kiani K 2015 Elastic wave propagation in magnetically affected double-walled carbon nanotubes *Meccanica* **50** 1003–26

[50] Han Q and Lu G 2003 Torsional buckling of a double-walled carbon nanotube embedded in an elastic medium *Euro. J. Mech.* A **22** 875–83

[51] Tounsi A, Benguedia S, Adda B, Semmah A and Zidour M 2013 Nonlocal effects on thermal buckling properties of double-walled carbon nanotubes *Adv. Nano Res.* **1** 1–11

[52] Benguediab S, Tounsi A, Zidour M and Semmah A 2014 Chirality and scale effects on mechanical buckling properties of zigzag double-walled carbon nanotubes *Composites* B **57** 21–4

[53] Shen H S and Zhang C L 2010 Torsional buckling and postbuckling of double-walled carbon nanotubes by nonlocal shear deformable shell model *Compos. Struct.* **92** 1073–84

[54] Shen H S and Zhang C L 2010 Nonlocal shear deformable shell model for post-buckling of axially compressed double-walled carbon nanotubes embedded in an elastic matrix *J. Appl. Mech.* **77** 041006

[55] Ghorbanpour Arani A, Roudbari M A and Kiani K 2016 Vibration of double-walled carbon nanotubes coupled by temperature-dependent medium under a moving nanoparticle with multi physical fields *Mech. Adv. Mater. Struct.* **23** 281–91
[56] Ke L L, Xiang Y, Yang J and Kitipornchai S 2009 Nonlinear free vibration of embedded double-walled carbon nanotubes based on nonlocal Timoshenko beam theory *Comp. Mater. Sci.* **47** 409–17
[57] Fang B, Zhen Y X, Zhang C P and Tang Y 2013 Nonlinear vibration analysis of double-walled carbon nanotubes based on nonlocal elasticity theory *Appl. Math. Model.* **37** 1096–107
[58] Kiani K 2014 Nonlocal continuous models for forced vibration analysis of two- and three-dimensional ensembles of single-walled carbon nanotubes *Physica* E **60** 229–45
[59] Kiani K 2014 In- and out-of- plane dynamic flexural behaviors of two-dimensional ensembles of vertically aligned single-walled carbon nanotubes *Physica* B **449** 164–80
[60] Kiani K 2016 Free vibration of in-plane-aligned membranes of single-walled carbon nanotubes in the presence of in-plane-unidirectional magnetic fields *J. Vib. Control.* **22** 3736–66
[61] Kiani K 2015 Nonlocal and shear effects on column buckling of single-layered membranes from stocky single-walled carbon nanotubes *Composites* B **79** 535–52
[62] Peddieson J, Buchanan G R and McNitt R P 2003 Application of nonlocal continuum models to nanotechnology *Int. J. Eng. Sci.* **41** 305–12
[63] Wang Q and Wang C M 2007 The constitutive relation and small scale parameter of nonlocal continuum mechanics for modelling carbon nanotubes *Nanotechnology* **18** 075702
[64] Wang C M, Zhang Y Y, Ramesh S S and Kitipornchai S 2006 Buckling analysis of micro-and nano-rods/tubes based on nonlocal Timoshenko beam theory *J. Phys. D: Appl. Phys.* **39** 3904
[65] Wang C M, Zhang Y Y and He X Q 2007 Vibration of nonlocal Timoshenko beams *Nanotechnology* **18** 105401